NASA Tech Briefs

National Aeronautics and Space Administration

September 1997
97-09

5 Electronic Components and Circuits

11 Electronic Systems

17 Physical Sciences

27 Materials

33 Computer Programs

37 Mechanics

45 Machinery

49 Fabrication Technology

53 Mathematics and Information Sciences

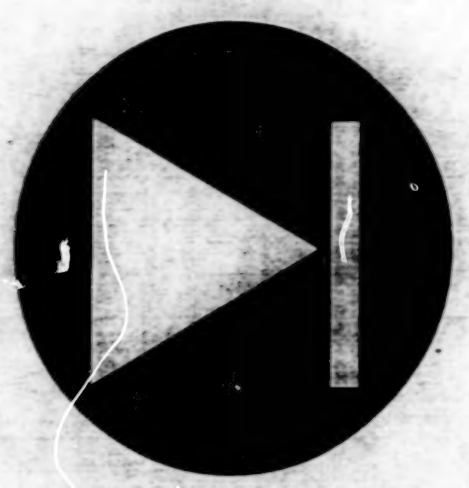

Electronic Components and Circuits

Hardware, Techniques, and Processes

7 Generalized Scattering Matrices for Quasi-Optical Circuits
8 High-Power Photodiodes for Microwave Fiber-Optic Links
9 Circuit Maintains Centering of a Laser Frequency Scan

Generalized Scattering Matrices for Quasi-Optical Circuits

Analysis of grid amplifiers and oscillators is unified with preexisting theory.

NASA's Jet Propulsion Laboratory, Pasadena, California

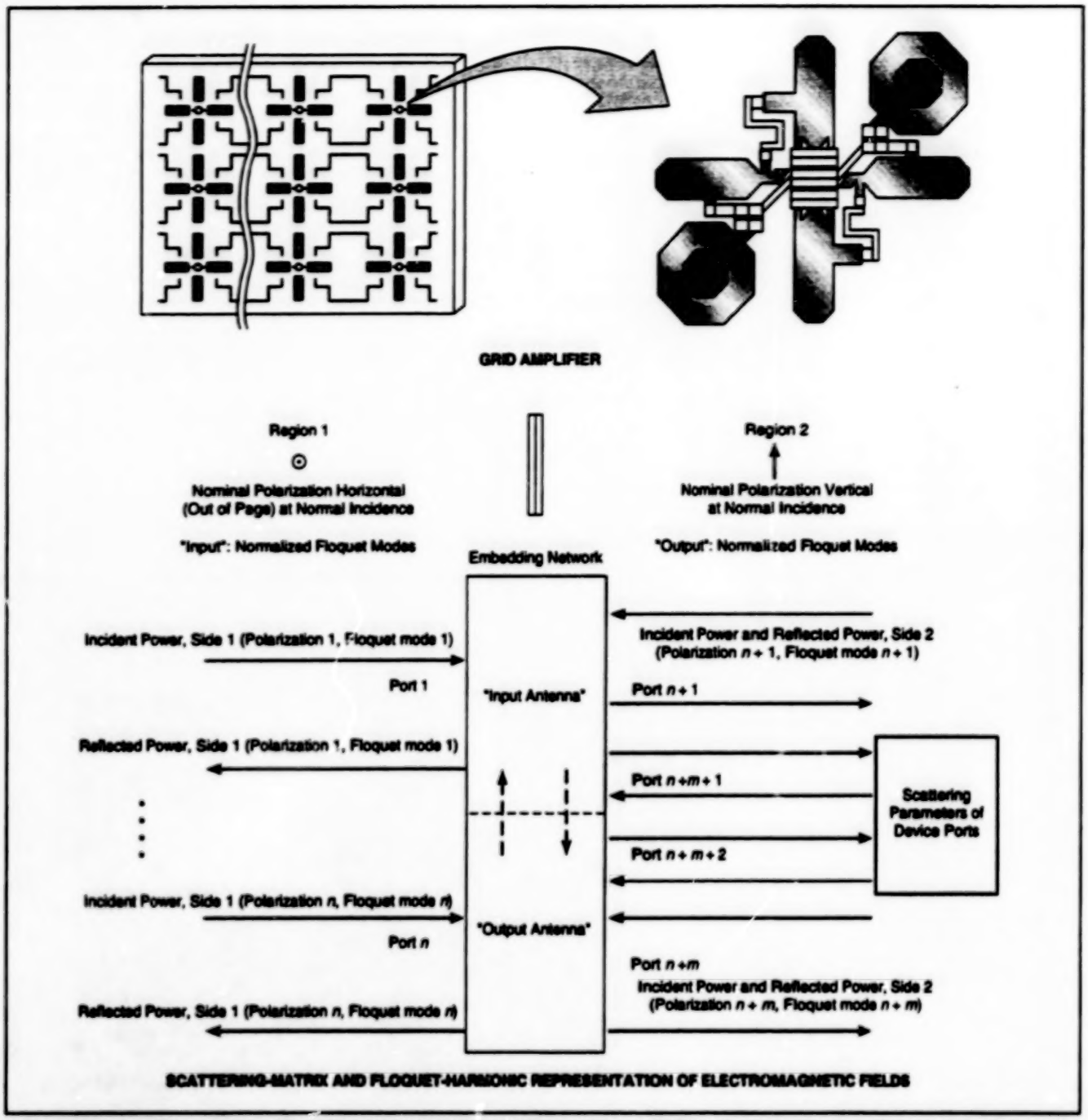

A Typical Grid Amplifier contains a differential pair of high-electron-mobility transistors (HEMTs), with input and output antennas nominally decoupled by orthogonality of their polarizations at normal incidence. The components of the electromagnetic field on both sides of the amplifier plane are represented by Floquet harmonics in the half spaces designated as regions 1 and 2.

A generalized-scattering-matrix approach provides a theoretical foundation for analysis and design of grid amplifiers and grid oscillators (periodic planar arrays of microwave amplifiers or oscillators with antennas, dc bias lines, and possibly other circuit elements). The generalized-scattering-matrix approach involves mathematical modeling that accounts for (1) the quasi-optical nature of electromagnetic fields that excite and are excited by the circuitry, (2) the periodicity of the circuitry, and (3) the parameters of solid-state devices in the circuits. This approach unifies the analysis and design of grid amplifiers and oscillators with preexisting amplifier theory, making it possible to design improved quasi-optical circuits for monolithic fabrication on single wafers. The generalized-scattering-matrix approach also provides means to deembed the parameters of an active device from transmission and reflection coefficients measured in a test of a single unit cell in a waveguide simulator; this deem-

3

bedding concept was described in "Device Deembedding From Waveguide Simulator Test" (NPO-19554) *NASA Tech Briefs*, Vol. 21, No. 2 (February 1997), page 32.

For purposes of this approach, the parameters of a semiconductor electronic device in a grid amplifier or oscillator are presented in the scattering-matrix ("S-parameter") format that is also used to represent the transmission and reflection properties of waveguides. (Each coefficient or S-parameter is a transmission or reflection coefficient indexed to an input and/or an output port.) The periodic nature of the grid amplifier or oscillator is incorporated into the mathematical model of the circuitry by use of a generalized scattering matrix, wherein the electromagnetic scattering characteristics of the array are modeled by use of Floquet harmonics, as though each such harmonic represented a port of the amplifier or oscillator array. These "ports" are combined with power-wave representations of the device ports in the grid plane. Magnetic and electric wall assumptions are not needed in this method. Furthermore, in the Floquet-mode representation, scattering matrices can be cascaded to model the effects of nonnormal incidence, of coupling between input and output antennas, and of substrates, superstrates, polarizers, dc bias lines, and other periodic structures.

The top part of the figure illustrates a typical grid amplifier. In each unit cell, the location of attachment between the horizontal dipole antenna and the gates of the transistors constitutes the input port, while the location of attachment between the vertical dipole and the drains of the HEMTs constitutes the output port. One seeks the generalized scattering matrix, S^{num}, that describes the periodic array. So that a single unit can be modeled readily, the array is assumed to be infinite. A unit cell is described in terms of the currents on its metallic surfaces. The scattered fields generated by these currents are expressed as Floquet harmonics, and each such harmonic is regarded as a port. To find S^{num}, the array is excited with an incident Floquet harmonic at one port, and the coefficients of the scattered harmonics in region 1 and region 2 are computed with all ports matched.

Since the infinite half spaces are inherently matched, it is necessary to match the device ports (the input and output ports mentioned above). First, for each port, one computes an input impedance, which is then used as the reference impedance for the location of the port. The scattering parameters between the incident Floquet harmonic ports and all the other ports, including device ports, are then found directly. The scattering parameters between device ports and Floquet harmonics are then computed from the symmetry of the generalized scattering parameters.

This work was done by Larry W. Epp of Caltech for **NASA's Jet Propulsion Laboratory**. *Further information is contained in a TSP [see page 1].*
NPO-19775

High-Power Photodiodes for Microwave Fiber-Optic Links

High-saturation-level PIN photodiodes are embedded in waveguide structures.

NASA's Jet Propulsion Laboratory, Pasadena, California

Optical waveguide geometry photodetectors with increased optical saturation powers are being developed for use in detecting analog signals that are transmitted through optical fibers with laser light that is modulated at microwave frequencies. Transmission of microwave signals through optical fibers offers tremendous improvements in both flexibility and loss due to the unique properties of optical fibers. However, significant losses can occur during the electrical-to-optical and optical-to-electrical conversions required at each end of the fiber-optic link. These conversion losses can be overcome through the use of a high-power laser and an external modulator at the transmitter and a high-speed, high-saturation power photodetector at the receiver. At present, the performance of these links is limited by the saturation power of the high-speed photodetectors; saturation produces a nonlinear electrical output at the receiver, which degrades the fidelity of the link.

To increase the optical saturation level of the detectors while preserving high electrical frequency response, the geometry and material layer compositions need to be chosen carefully. First, the optical waveguide geometry is selected, as it provides the ability to achieve both high-speed operation and good optical-to-electrical conversion efficiency (see Figure 1). This results from the ability to use a thin layer of absorbing material, which maximizes the speed of the detector by minimizing the transit time for the photogenerated electrical signals (electrons with negative charge and holes with positive charge). Ideally, each absorbed photon creates a single electron-hole pair that escapes the detector due to the applied electric field. The conversion efficiency of the detector is maintained through the use of the optical waveguide geometry, which confines the incident optical signal within the detector and forces a continual interaction of the light with the thin absorbing layer as the light travels down the length of the detector. The interaction length required for complete absorption of the light deter-

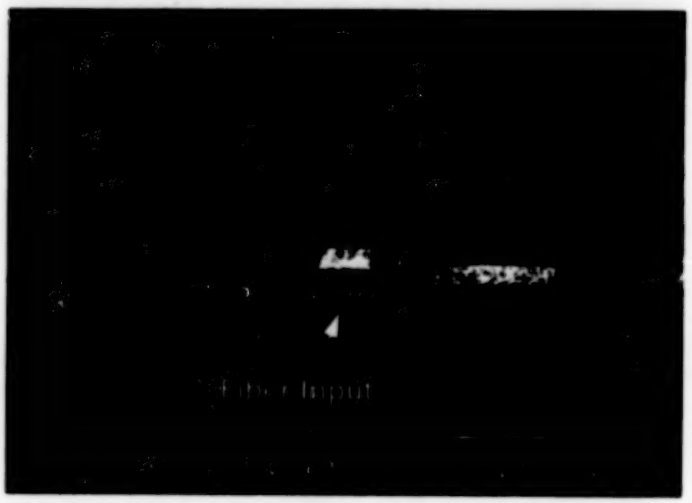

Figure 1. Scanning Electron-Beam Microscope (SEM) image of a cleaved-facet waveguide PIN photodetector is shown mounted for testing.

mines the length of the waveguide photodetector. Next, while the material layer composition of the positive/intrinsic/negative (PIN) detector is chosen to create the optical waveguide, at the same time this creates energy steps or barriers for the photogenerated electrons and holes to overcome in their transit out of the absorbing layer and out to the electrical terminals of the detector.

During operation, the device is reverse biased such that the applied electric field pulls the holes out of the positive side of the detector and the electrons out of the negative side of the detector. Due to the different effective masses of the electrons and holes, an asymmetric material design has been utilized to minimize these barriers for both the electrons and holes while maintaining an effective optical waveguide, and a comparison has been made to a standard symmetric material design. Overall dimensions of the waveguide detector have been chosen to limit parasitic resistance-capacitance and transit-time effects for operation beyond 40 GHz.

The standard symmetric waveguide photodiode contains InP and InGaAsP on both the p-doped and n-doped sides of the intrinsic InGaAs absorbing layer, with all of the material layers lattice matched to the semi-insulating InP substrate. The asymmetric waveguide photodetector replaces the InP and InGaAsP on the p-doped side with lattice matched InAlAs and InAlGaAs material layers that provide much smaller energy barriers for the photogenerated holes, while still maintaining the proper optical waveguiding characteristics.

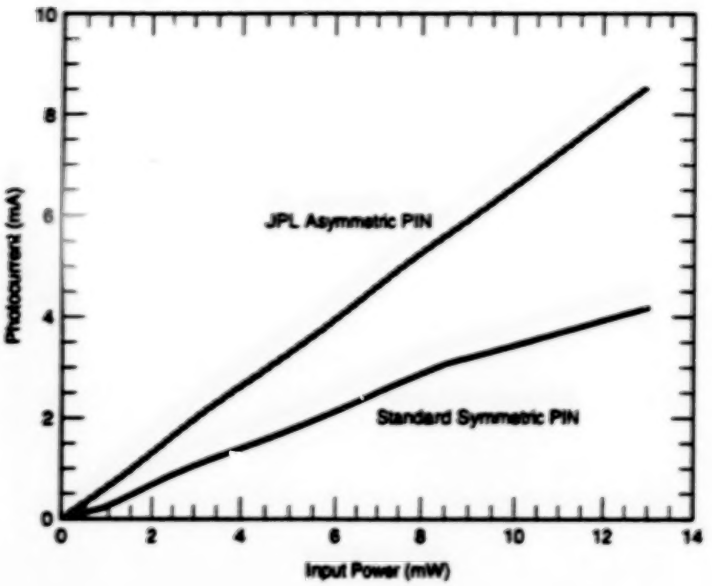

Figure 2. Comparison of the Responsivity of standard and asymmetric waveguide PINs was measured at a bias of –3 V.

Prototypes of both the symmetric and asymmetric devices have been made and tested, with both showing excellent electrical and dark-current properties. Uniform responsivity was obtained from both devices for applied biases between +0.25 and –5 V. Responsivity at small positive voltages indicates a significant built-in field due to the p and n regions and implies that these devices may be operated at relatively low bias levels. A significant improvement in the efficiency and linearity of the asymmetric design was observed (see Figure 2). A linear variation of photocurrent with incident optical power was observed for photocurrents over 8 mA for the asymmetric design. At present, this measurement is limited by the output power of the laser.

This work was done by Timothy A. Vang, Lawrence J. Davis IV, and Sam Keo of Caltech for **NASA's Jet Propulsion Laboratory**. *Further information is contained in a TSP [see page 1].*
NPO-19666

Circuit Maintains Centering of a Laser Frequency Scan

Drift in the nominally steady component of frequency offset is corrected automatically.

NASA's Jet Propulsion Laboratory, Pasadena, California

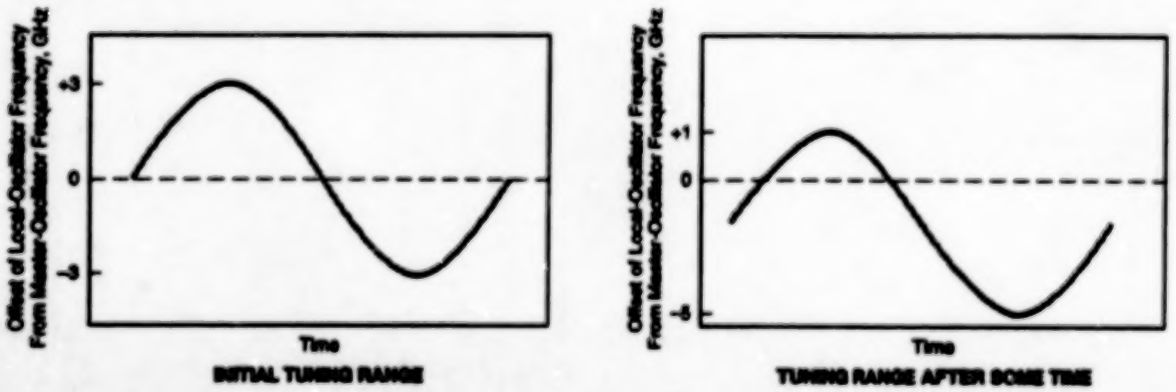

Figure 1. The Frequency Scan Is Sinusoidal, with an amplitude of 3 GHz. The scan is required to be centered at the master-oscillator frequency, but thermal, aging, and other effects can cause the central frequency to drift.

5

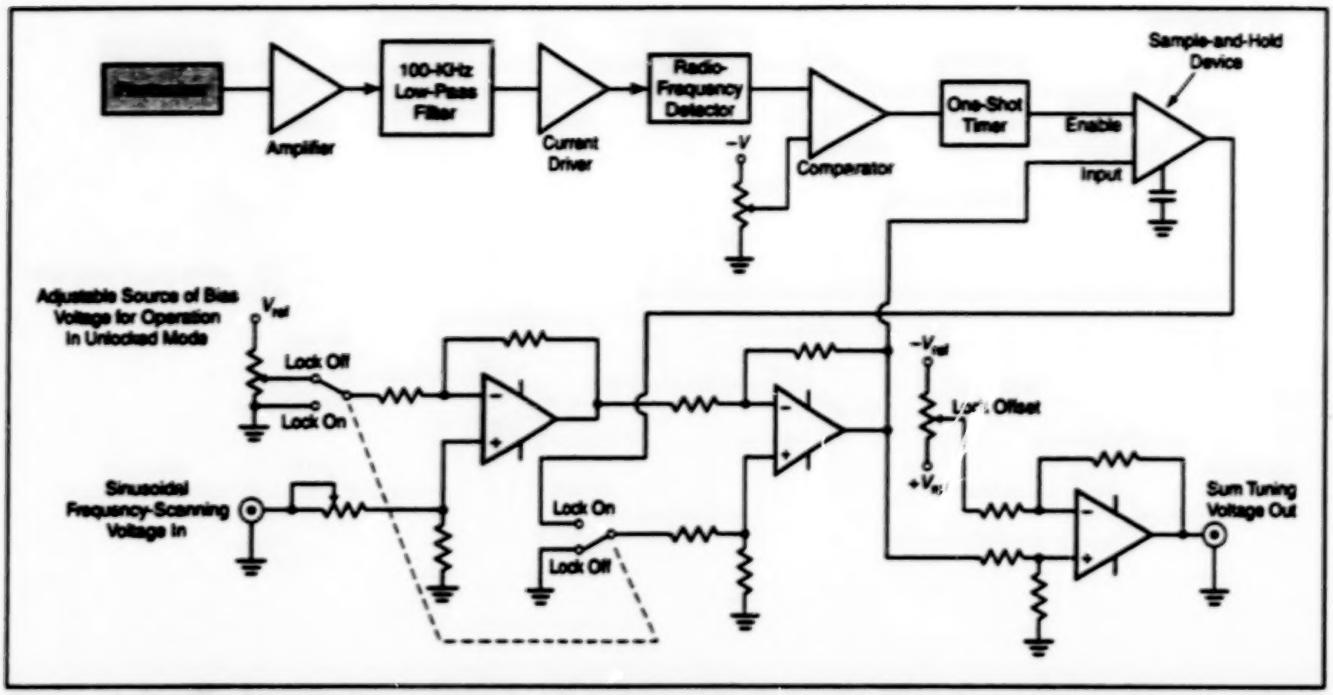

Figure 2. This Simplified Schematic Diagram shows the major functional blocks of a circuit that adjusts the dc component of the tuning voltage to lock the central local-oscillator frequency to the master-oscillator frequency. Optionally, the lock frequency can be offset somewhat from the master-oscillator frequency. The circuit can also optionally be switched to operate in a non-frequency-locking mode.

An electronic circuit maintains centering of a ±3-GHz frequency scan of a local-oscillator laser in a Doppler lidar system. The need for such a circuit arises as follows: In the Doppler lidar system, the frequency scan of the local-oscillator laser involves the generation of (1) a sinusoidally varying tuning voltage superimposed on (2) a dc tuning voltage. The sum tuning voltage is applied to a piezoelectric transducer that adjusts the length of the local-oscillator-laser cavity and thereby changes the local-oscillator frequency. The frequency scan is required to be symmetrical about the frequency of a master-oscillator laser, but in the absence of corrective action, the frequency scan becomes asymmetrical because the central frequency of the scan drifts gradually (see Figure 1). The overall function of the present circuit, described in more detail below, is to periodically adjust the dc tuning voltage to keep the frequency scan centered at the master-oscillator frequency.

The circuit (see Figure 2) includes a photomixer detector, on which small samples of the master- and local-oscillator laser beams are incident. The mixer output consists primarily of a beat note between the local- and master-oscillator signals. The beat note is amplified by a factor of 10, then sent through a low-pass filter with a cutoff frequency of 100 kHz. The net effect of the amplification and low-pass filtering is to generate a burst signal at frequencies < 100 kHz whenever the beat note passes through zero frequency; that is, whenever the local-oscillator frequency passes through the master-oscillator frequency.

The burst signal is fed to a radio-frequency detector, which converts the burst into a voltage spike. A comparator converts the voltage spike into a clean pulse, which triggers a one-shot timer. The one-shot timer engages a sample-and-hold device, which samples the instantaneous sum tuning voltage. Because the timing pulse is initiated whenever the local-oscillator frequency crosses the master-oscillator frequency, the voltage held by the sample-and-hold device is the tuning voltage that causes the local-oscillator frequency to equal the master-oscillator frequency. The dc component of the tuning voltage is reset to this held voltage. Thus, twice during each frequency scan (at the two frequency-crossover points), the dc component of the tuning voltage is adjusted to reset the central frequency of the scan to the master-oscillator frequency.

This work was done by Carlos Esproles of Caltech for **NASA's Jet Propulsion Laboratory.** *Further information is contained in a TSP [see page 1].*

NPO-20040

Electronic Systems

Hardware, Techniques, and Processes

13 Optical Encryption of Images for Data-Transmission Security
13 Improved Multilayer Optical Memory System
14 Optical Monitoring of Deflections of Compressor Blades
15 Photonic Processing of Multigigahertz Signals

Optical Encryption of Images for Data-Transmission Security

Phase-scrambling in optical fibers would provide the equivalent of long encryption keys.

NASA's Jet Propulsion Laboratory, Pasadena, California

In a proposed scheme for enhancing privacy in the digital transmission of images, each image would be encrypted optically (while still in its analog form) before digitization and transmission. In the receiver, the digital image data would be used to reconstruct the encrypted analog image, and this image would be decrypted optically. The analog encryption and decryption could be performed instead of, or in addition to, digital encryption and decryption. Of course, one of the advantages of optical analog encryption and decryption would be the inherent high-speed, massively parallel nature of optical processing.

The analog encryption would be initiated by launching a beam of light containing the image information into a multimode optical fiber (see figure). During propagation along the fiber, the phases of the wavefronts carrying the image information would become scrambled. Consider the practicality of measuring all the wavelength, phase, amplitude, and polarization components of the light emerging from the output end of the optical fiber, computing all the waveguide modes that can propagate in the multimode optical fiber, and computing the corresponding coefficients needed to unscramble the image information in the emerging light. It is not practical to do these things, but even if it were, the large number of the aforementioned components, modes, and coefficients would place digital computational unscrambling beyond the reach of current technology; the security of encryption would be comparable to that of digital encryption with a key of length $>10^6$, and possibly several orders of magnitude beyond that. In contrast, digital encryption keys in current use typically have lengths of 100 or less.

The only practical way to decrypt the encrypted analog image would be to reverse the phase-scrambling process optically. To make this possible, a beam of light carrying no spatial image information would be sent through the fiber and the emerging beam would be used to make a hologram that would embody the phase-scrambling information. Thereafter, the hologram would be placed in the path of the beam of light containing the reconstructed scrambled image to reverse the phase-scrambling process and thus recover the original image. It should be easy to construct optical-fiber/hologram scrambler/descrambler pairs such that each pair provided the equivalent of a unique, highly secure code.

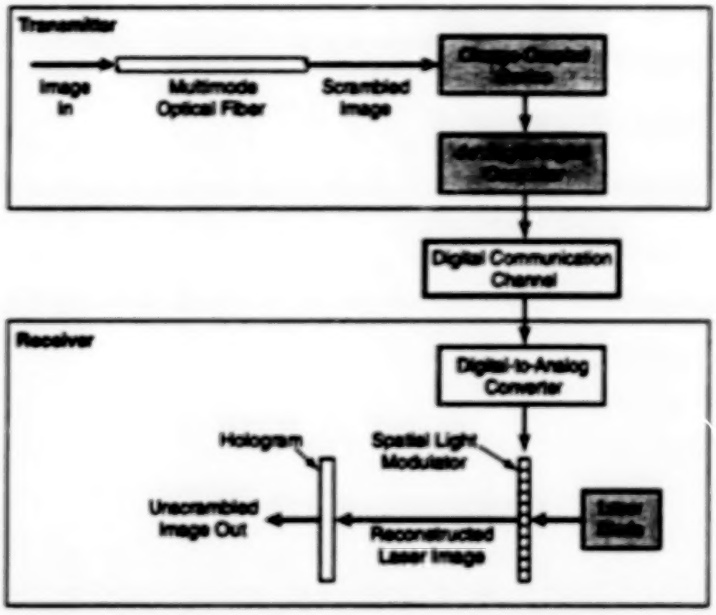

The Input Image Would Be Scrambled Optically in the multimode optical fiber prior to transmission. After reconstruction of the scrambled image in the receiver, the image would be unscrambled optically by use of a hologram previously made from the optical fiber.

This work was done by Deborah L. Jackson and Chien C. Chen of Caltech for **NASA's Jet Propulsion Laboratory.** *Further information is contained in a TSP [see page 1].*

In accordance with Public Law 96-517, the contractor has elected to retain title to this invention. Inquiries concerning rights for its commercial use should be addressed to

Technology Reporting Office
JPL
Mail Stop 122-116
4800 Oak Grove Drive
Pasadena, CA 91109
(818) 354-2240

Refer to NPO-19574, volume and number of this NASA Tech Briefs *issue, and the page number.*

Improved Multilayer Optical Memory System

Improvements would be made in readout optics, identification of layers, and compositions of layers.

Lyndon B. Johnson Space Center, Houston, Texas

A proposed optoelectronic memory system based on a multilayer read-only optical disk would incorporate three improvements over a previous system of this type. As in the previous system, binary data would be stored in the spatially varying reflectivities of spiral tracks in multiple layers in the disk, light from a laser would be focused onto a selected layer, and the data stored in that layer would be read out via the reflected light. The proposed system would differ from the previous system in the readout optics, the method of identification of layers, and the compositions of the layers.

The figure is a greatly simplified schematic diagram of the readout optics. The improvement in the readout optics would

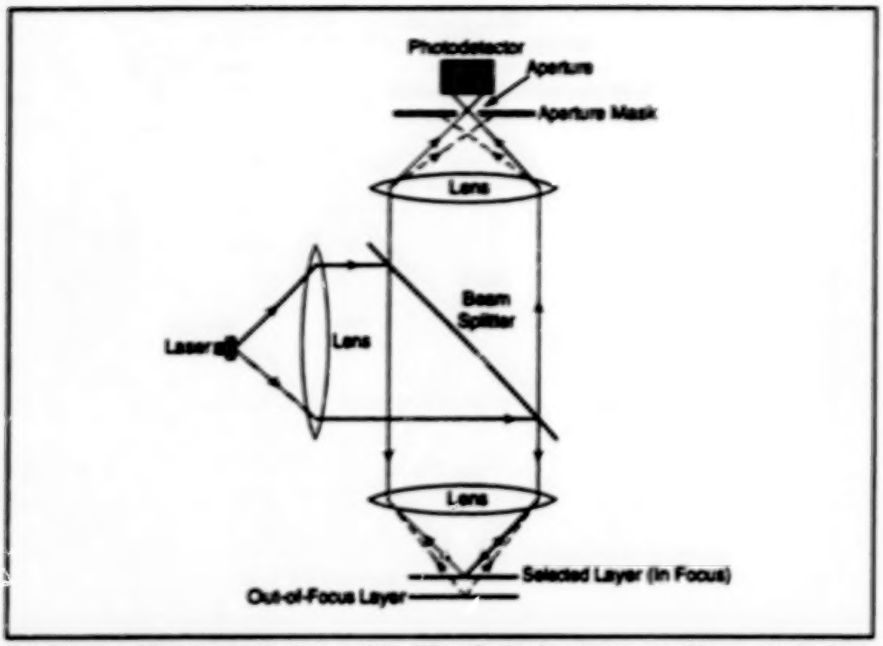

The Aperture Mask would block most of the light reflected from layers out of focus; only the light reflected from the selected layer would be focused into the aperture and thereby allowed to pass unimpeded to the photodetector.

consist of the addition of an aperture at the spot onto which light reflected from the illuminated spot in the selected data-storage layer would be focused. The aperture would be large enough to allow a substantial portion of the desired focused light reflected from the selected layer to pass through to the photodetector. The aperture would also be wide enough to provide sufficient range for a focus-control subsystem. At the same time, the aperture would be small enough so that the aperture mask would block most of the out-of-focus light reflected from the other layers, so that the aperture would help to prevent readout crosstalk between layers.

Previously, the data-storage layers in a disk were identified via codes incorporated into the stored data by use of additional bits. In the proposed system, there would be no need for these codes and the extra bits. Instead, upon insertion of a new disk in the proposed system, the optical readout head would be set at the top of its travel, then scanned downward until it encountered the uppermost layer in the disk. It would read the directory of that layer, then scan down to the next layer and scan its directory, and so on, down to the lowermost layer. The system would track its location by counting the passage of layers. Thereafter, upon a request by the user for information in a given layer, the optical readout head would be scanned upward or downward from its present location, counting the passage of layers until it reached the given layer.

In this scheme, it would be desirable to have redundant information to verify the identity of the layer as determined by counting. This is because, for example, a mechanical shock during scanning could cause a layer to be skipped. In the proposed system, the redundant layer-identification information would lie in the average amplitude of the readout signal; the average reflectivity of each layer would have a unique value, so that the average level of the readout signal from each level would have a unique value. During the initial downward scan through a new disk, the system could record the average readout signal from each layer. During subsequent readout from that disk, the system could compare the average readout signal with the recorded value for the layer being read to verify the identity of the layer.

Previously, it had been proposed to store data in contrasting dielectric layers to avoid the absorption losses that are associated with the use of metallic films as reflective elements. However, research has since shown that it may be desirable to use metallic films to obtain high (≈50 percent) reflectivities. By making these films thin enough (≈10 nm thick), it should be possible to minimize absorption losses. In particular, gold appears to be the material of choice for enhancing the reflectivity of the second-deepest layer. The deepest layer could be made of aluminum and it could be made relatively thick because absorption is not a concern for that layer.

This work was done by James Strickler of Strickler Optical Technology, Inc., for **Johnson Space Center**. *Further information is contained in a TSP [see page 1].*
MSC-22452/53/54

Optical Monitoring of Deflections of Compressor Blades

Fiber-optic sensors indicate deflections and blade-tip clearances in real time.

Lewis Research Center, Cleveland, Ohio

A compact instrumentation system has been developed for use in remote monitoring of the vibrational modes and static deflections of compressor blades, especially in aircraft engines. The system includes state-of-the-art integrated fiber-optic sensors and a state-of-the-art electronic processing subsystem with parallel-processing capability. Together, the optical and electronic subsystems provide simultaneous, near-real-time measurements of the deflections and tip clearances of compressor blades with timing resolution of 5 nanoseconds.

Each fiber-optic sensor tip contains transmitting and receiving optics needed to measure blade arrival. These optics include a gradient-index fiber lens fused to a monomode optical fiber for delivering, to a passing blade tip, a spot of coherent light about 50 μm wide. An array of high-numerical-aperture fibers gathers diffusively scattered light and transmits it to avalanche photodiodes, the outputs of which are processed in the electronic subsystem to extract the required information. Several fiber-optic sensor tips positioned along the blade chord provide measurements containing information on vibrational modes.

This work was done by Anatole P. Kurkov of **Lewis Research Center** *and Harbans S. Dhadwal, Romel Khan, and Ali Mehmud of the State University of New York at Stony Brook. Further information is contained in a TSP [see page 1].*

Inquiries concerning rights for the commercial use of this invention should be addressed to the Patent Counsel, Lewis Research Center [see page 1]. Refer to LEW-16068.

Photonic Processing of Multigigahertz Signals

Optoelectronic heterodyning is among the techniques used.

NASA's Jet Propulsion Laboratory, Pasadena, California

Some disparate elements of fiber-optic, electro-optical, and optoelectronic technology have begun to coalesce in the development of a unified partly photonic, partly electronic approach to the processing (including generation, transmission, and reception) of electromagnetic signals at frequencies of about 1 to 300 GHz. Photonic technology now appears to be a viable alternative to traditional electronic-only technology for realizing the building blocks of advanced communication systems that will exploit the advantages (light weight, low loss, compactness, large bandwidth) of fiber-optic transmission media, compared to transmission of multigigahertz signals over metallic waveguides.

The figure schematically illustrates one example of an application following this approach. The two lasers shown at the left side of the figure are narrow-band units that are tuned so the difference between output frequencies equals a desired microwave or millimeter-wave heterodyne beat frequency, e.g., 30 GHz. A stable electronic reference signal can be used to maintain phase coherence between the lasers. The outputs of these lasers are combined in a fiber-optic coupler, then amplitude modulated by a modulated carrier signal that differs in frequency from the first-mentioned heterodyne beat frequency by a relatively small amount (e.g., 300 MHz) that equals the desired intermediate frequency to be generated at the receiving end. The modulation on the 30.3-GHz modulating carrier signal is the information signal to be downconverted and transmitted.

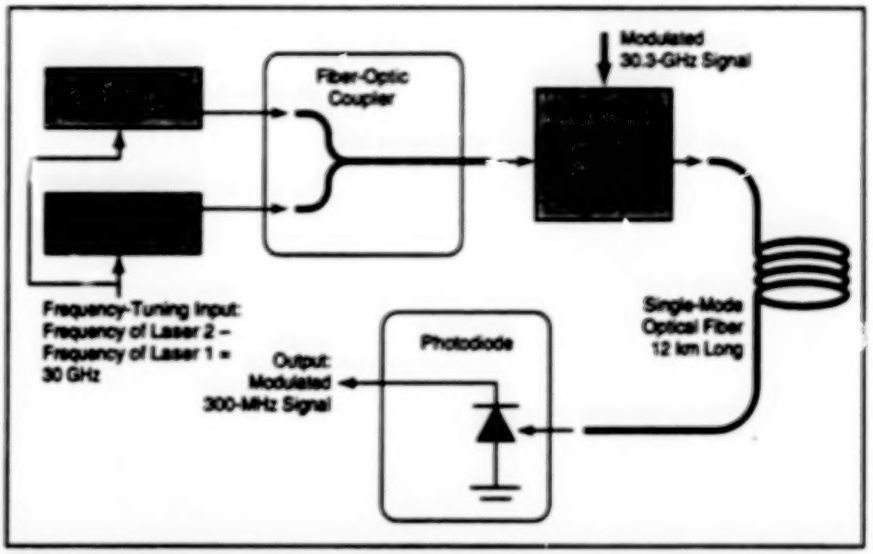

This Photonic/Electronic System is a simple example of how a system effects (1) up-conversion of electrical signals to modulated optical signals, (2) transmission along an optical fiber, and (3) down-conversion of optical to electrical signals. Other architectures are possible for up-conversion, phase modulation, and the like.

The combined, modulated laser beams are transmitted along an optical fiber (e.g., 12 km long) to a receiver, where the optical signal is detected. The heterodyne action of the detection process yields the desired downconverted output signal, which is an intermediate-frequency (300-MHz) carrier modulated by the information signal. Previously, a complex system of several stages of electronic downconverters employing electronic mixers, filters, and amplifiers would be required to perform this function.

This work was done by Ronald T. Logan, Jr., George F. Lutes, and X. Steve Yao of Caltech for **NASA's Jet Propulsion Laboratory**. *Further information is contained in a TSP [see page 1].*

In accordance with Public Law 96-517, the contractor has elected to retain title to this invention. Inquiries concerning rights for its commercial use should be addressed to

Larry Gilbert, Director
Technology Transfer
California Institute of Technology
Mail Code 315-6
Pasadena, CA 91125
(818) 395-3288

Refer to NPO-19437, volume and number of this NASA Tech Briefs *issue, and the page number.*

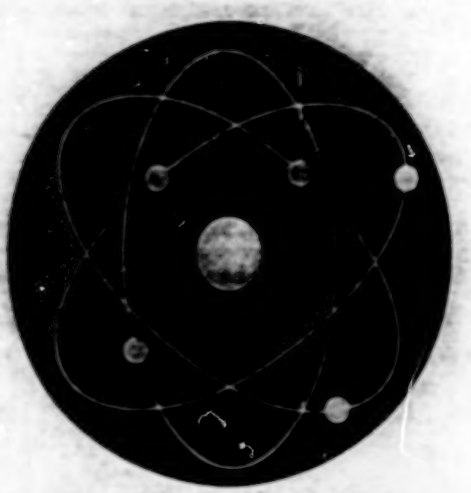

Physical Sciences

Hardware, Techniques, and Processes

19 Miniature Inside-Out EPR Spectrometers
20 Improved Noncontact Techniques for Measuring Volumes of Drops
21 Laser Vibrometry of Supported Membranes
22 Laser Extensometer for Noncontact Measurement of Strain
23 Deicing-Fluid and Ice-Thickness Monitor for Aircraft
24 Air-Sampling System Measures Dew Point in a Wind Tunnel
25 Parallel-Processing Program for Assimilation of Weather Data

Miniature Inside-Out EPR Spectrometers

Large samples could be probed from surface or borehole locations.

NASA's Jet Propulsion Laboratory, Pasadena, California

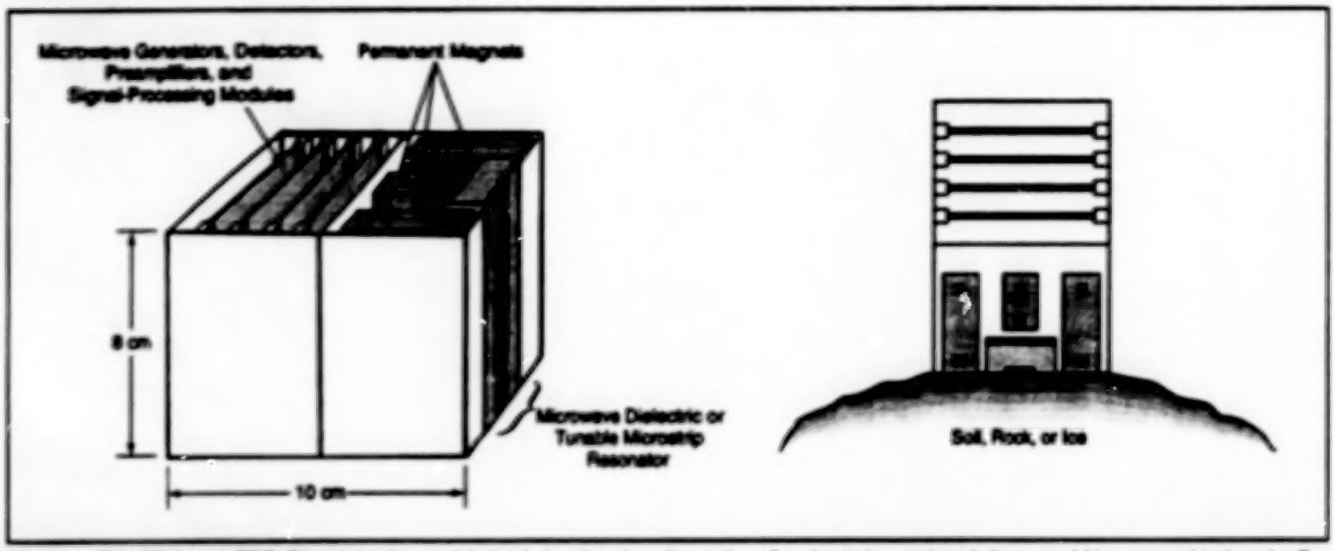

Figure 1. This Miniature EPR Spectrometer would simply be placed on the rock, soil, or ice to be analyzed; there would be no need to break off a small sample and insert it in a sample chamber.

Miniature electron-paramagnetic-resonance (EPR) spectrometers have been proposed for use in field analysis of soil, rocks, and ice. These instruments would incorporate some of the features of the ones described in "Portable Wide-Band EPR Spectrometers" (NPO-19532) *NASA Tech Briefs*, Vol. 21, No. 3 (March 1997), page 56. The unique feature of the proposed EPR spectrometers would be "inside-out" sampling-head configurations that would cause sampling dc magnetic and microwave-frequency fields to reach out to small regions outside the sampling heads.

To operate a conventional laboratory EPR spectrometer, it is necessary to place the sample to be analyzed in a microwave cavity with a small sample volume (typically, no more than 2 cm³). However, preparation and insertion of small samples can be difficult under field conditions. The proposed instruments would make it unnecessary to prepare small samples; instead, one could utilize the external sampling fields to probe large rocks, soil banks, and ice from surface or borehole locations.

The "inside-out" designs of the sampling heads of the proposed EPR spectrometers would be derived from similar designs of sampling heads of some oil-well logging nuclear-magnetic-resonance (NMR) spectrometers. Each sampling head would comprise permanent magnets and a microwave dielectric or tunable microstrip resonator. Figure 1 illustrates a typical unit for surface sampling; in this case, it would be possible to incorporate the sampling head and the associated electronic circuitry into one compact package. Figure 2 illustrates a typical unit for borehole sampling; in this case, the requirement for compactness to fit in the borehole would dictate that some of the electronic circuitry be housed above ground.

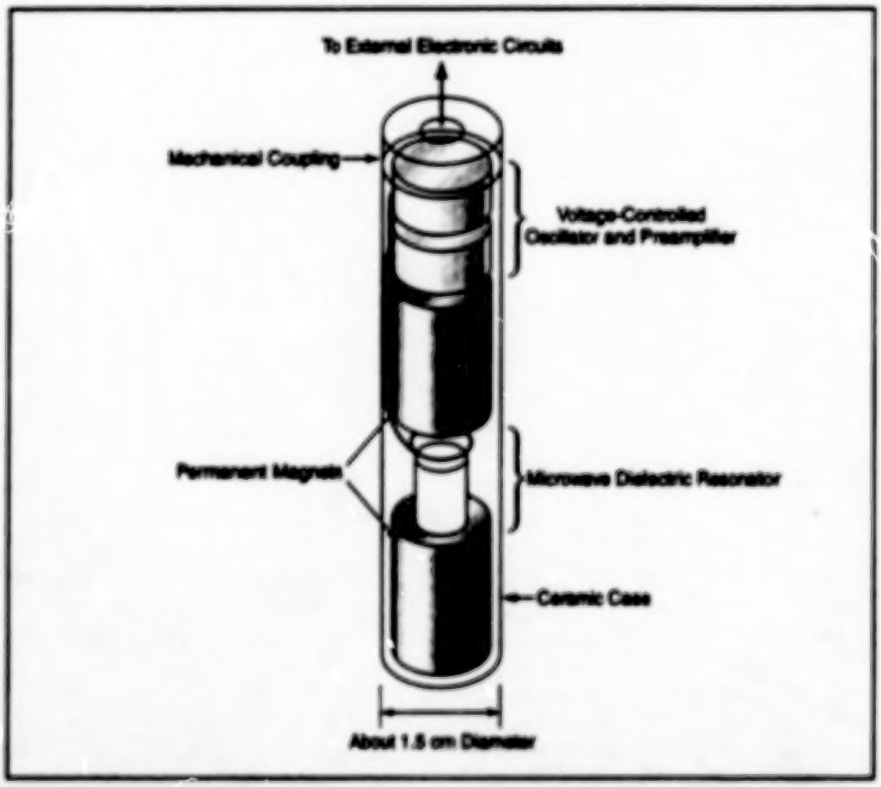

Figure 2. Lowered into a Borehole or simply pushed into soil, this miniature EPR could provide information on some aspects of chemical composition (e.g., concentrations of paramagnetic transition metals) as a function of depth.

This work was done by Soon Sam Kim and Narayan R. Mysoor of Caltech for NASA's Jet Propulsion Laboratory. Further information is contained in a TSP [see page 1].

NPO-19660

Improved Noncontact Technique for Measuring Volumes of Drops

Electrostatic levitation offers advantages over electromagnetic levitation.

NASA's Jet Propulsion Laboratory, Pasadena, California

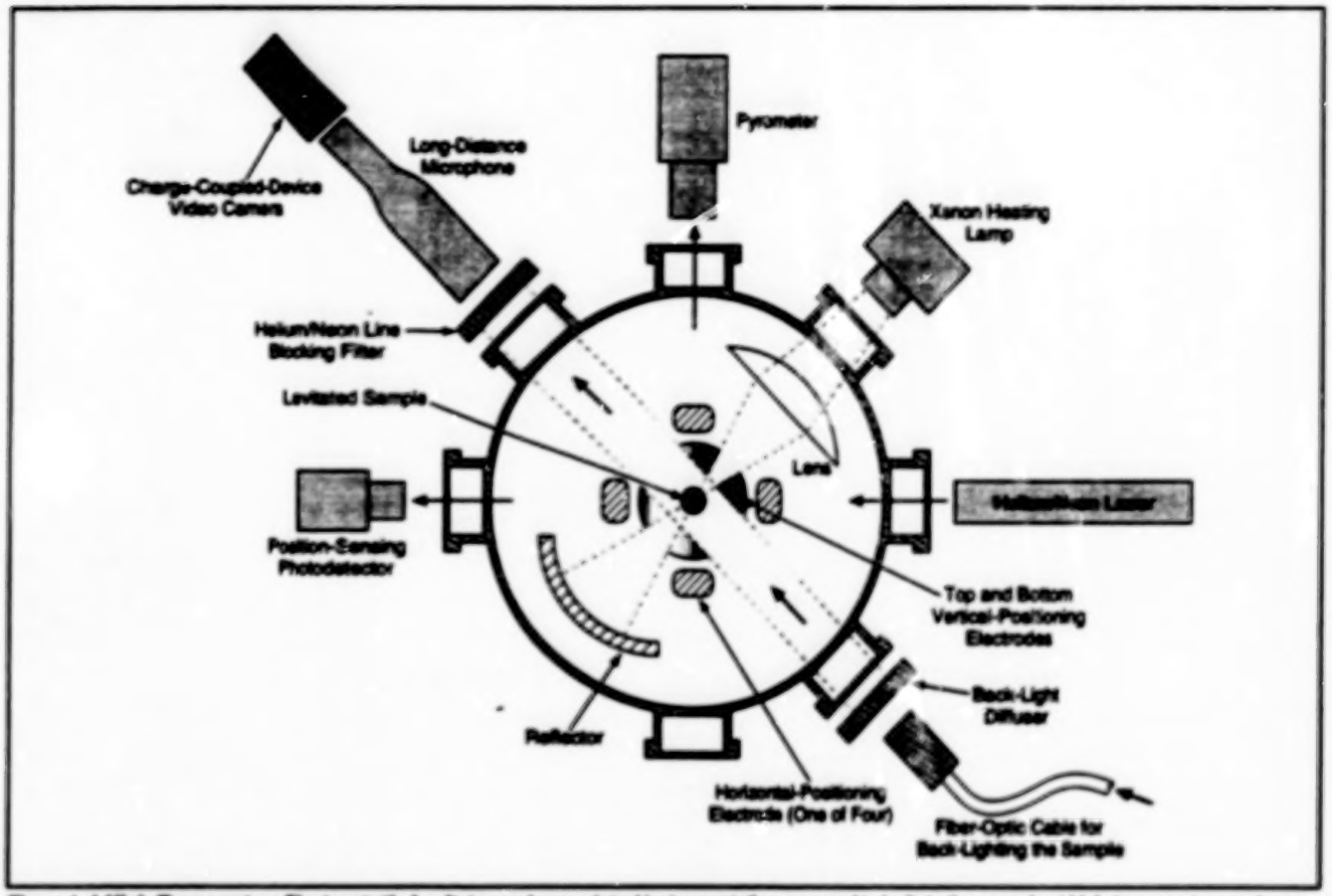

Figure 1. A High-Temperature Electrostatic Levitator and associated instrumentation are used to levitate the sample at high temperature and measure its volume. The volume of the sample is computed from the video image.

An improved noncontact technique provides accurate measurements of the volumes of small (diameter 2 to 3 mm) liquid and solid material samples at high temperatures. The technique is suitable for determining the densities and coefficients of thermal expansion of metals, semiconductors, and other materials that are required to be kept pure during measurement. In this technique, a sample is observed and heated while it is levitated electrostatically in a high vacuum (see Figure 1). The observation includes recording a video image of the sample. The image is then digitized, and the digital image data are processed to determine the volume of the sample.

The most closely related noncontact technique used heretofore to measure the volumes of small samples involves photographing samples that are levitated electromagnetically. Electromagnetic levitation imposes several limitations on the desired measurement capability: (1) In a liquid sample, stirring caused by the eddy currents tends to distort the shape of the sample severely, so that the measurement of the volume of the sample becomes complicated and inaccurate. (2) The sample material must either be inherently electrically conductive or else be made electrically conductive by addition of electrically conductive material, which constitutes an undesired impurity; therefore, almost all nonconductors and semiconductors are excluded from measurement. (3) The electromagnetic-levitation apparatus includes coils wound closely around the sample, making it difficult to acquire an image of the sample. (4) Heating and levitation are strongly coupled, so that it is very difficult to measure the volume of a material at a low temperature. The electrostatic levitation technique overcomes all of these disadvantages.

In the improved technique, the position of the sample is controlled actively, and can be maintained stable within 10 μm. The configuration of the electrostatic-levitation electrodes and of the resulting electric field is such as to induce the sample to stay axisymmetric when it is in liquid form, and the video camera views the sample along a horizontal line through the vertical axis of symmetry; therefore, only a single video image provides all the information needed to compute the volume of the sample.

The digitized image data are processed by algorithms similar to those used to analyze the shapes of pendant drops to determine their surface tensions. First, an edge-detection algorithm generates the coordinates of about 400 edge points. These coordinates are then refined in a process that involves analysis of gradients of image intensity in the vicinities of these points. Next, a least-squares best fit is made between the refined edge coordinates and a sixth-order series of axisymmetric spherical

harmonics. Then the volume (V) is computed straightforwardly from

$$V = (2\pi/3)\int_0^{\pi}\left[R(\theta)\right]^3 \sin\theta\, d\theta$$

where θ denotes the polar angle and $R(\theta)$ denotes the local radius as expressed by the finite series.

If the observation and the computation of volume of a given sample is repeated for a sequence of temperatures, then the coefficient of thermal expansion of the sample material can be computed from the measured volumes and temperatures. If mass of the sample is known, then its density as a function of temperature can also be determined. The technique has been demonstrated on specimens of nickel at temperatures above and below the melting temperature (see Figure 2).

This work was done by Sang K. Chung, David Thiessen, and Won-Kyu Rhim of Caltech for **NASA's Jet Propulsion Laboratory.** *Further information is contained in a TSP [see page 1].*
NPO-19779

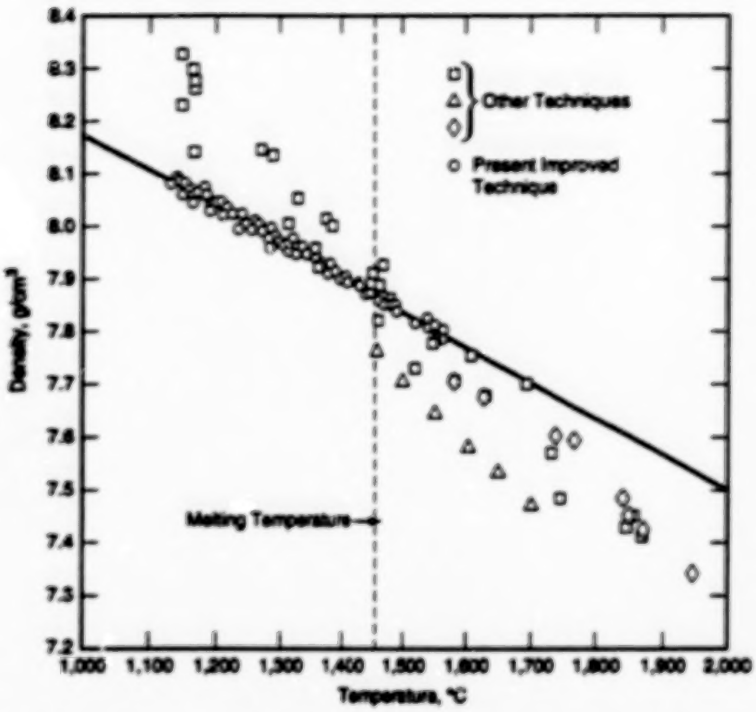

Figure 2. The Density of Nickel vs. Temperature around the melting temperature was determined by the technique described in the text, and is shown here in comparison with similar determinations by other techniques.

Laser Vibrometry of Supported Membranes

Stresses can be computed from modal responses.

NASA's Jet Propulsion Laboratory, Pasadena, California

A laser-vibrometric apparatus yields measurement data from which one can compute stresses in thin, small-area membranes supported rigidly around their edges. The apparatus was designed especially for testing amorphous (in the sense of noncrystalline) metallized composite membranes like those used in x-ray lithography masks, millimeter-wave transmission lines, and microelectromechanical devices. Stress-measuring techniques based on x-ray diffraction or Raman spectroscopy are not effective when applied to amorphous membranes, but laser vibrometry can be used without regard to the presence or absence of crystalline microstructure. In addition, laser vibrometry can be used to characterize dynamic (modal) responses, and is applicable to irregularly shaped membranes.

In the apparatus (see figure), a frame or substrate that supports a specimen membrane is mounted on a specimen holder in front of a loudspeaker, which is driven at controlled amplitude and frequency to excite vibrations in the membrane. A laser vibrometer measures the vibrational response (amplitude and phase of displacement as a function of frequency) at selected locations on the membrane. A digital signal analyzer preprocesses the output of the laser vibrometer to furnish frequency, displacement, and phase information to a computer for further analysis. To obtain calibration data for use in accounting for the frequency response of the loudspeaker, the specimen can be removed and replaced by a microphone to measure the acoustic pressure as a function of frequency.

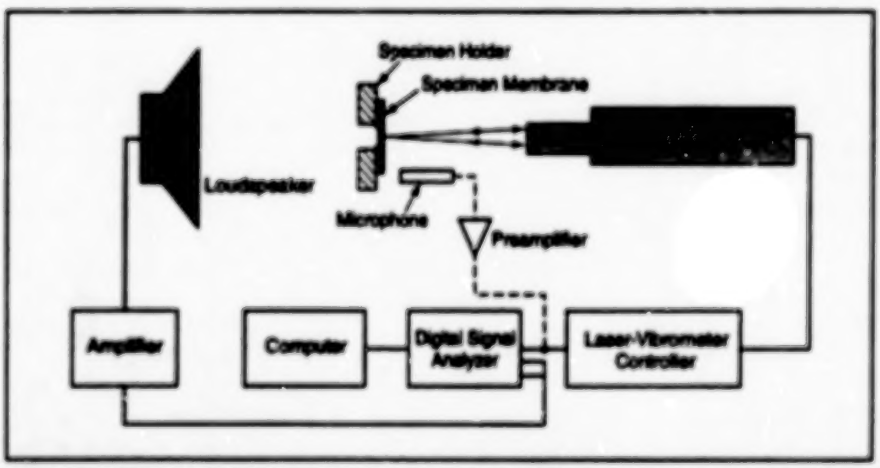

The Laser Vibrometer interferometrically measures the displacement at one spot on the vibrating membrane. Measurements are taken at various spots and frequencies to obtain data on vibrational modes.

Typically the analysis is directed toward identification of vibrational modes and their resonance frequencies. The resulting data can then be used to compute stresses. For example, in the case of a homogeneous rectangular membrane of dimensions L_x by

L_y and mass density ρ subject to uniform biaxial tensile stress σ, one can compute the stress from

$$\sigma = \frac{2\rho f_{mn}^2}{\left[(m/L_x)^2 + (n/L_y)^2\right]}$$

where m and n are integers that denote a vibrational mode and f_{mn} is the resonance frequency of that mode. In the case of an inhomogeneous and/or irregularly shaped membrane, the interpretation of measurement data is more complex, involving finite-element analysis to match predicted vibrational responses to the measured responses at all frequencies and locations of interest.

This work was done by Abhijit Biswas of Caltech for **NASA's Jet Propulsion Laboratory**. *Further information is contained in a TSP [see page 1].*
NPO-19751

Laser Extensometer for Noncontact Measurement of Strain

Strains in hot specimens can readily be measured in real time.

Lewis Research Center, Cleveland, Ohio

A laser extensometer provides noncontact measurements of strains, which could be steady or varying with time. This instrument is relatively easy to use and is especially well suited for measuring strains during tensile and fatigue tests of material specimens at temperatures up to 2,000 °F (1,100 °C). It is not necessary to prepare the surface of a specimen, nor is it necessary to place any part of the instrument in a hot test environment. Instead, this instrument is mounted on a tripod, facing the specimen (if necessary, through a test-chamber window) from a standoff distance of 8 in. (20 cm).

The laser extensometer is based on an interferometric principle that involves spatial and temporal heterodyning via a unique combination of techniques related to those of laser velocimetry and speckle metrology. The laser extensometer (see figure) includes a stabilized, two-frequency (Zeeman-split), helium/neon laser that produces two beams with orthogonal polarizations and with frequencies that differ by precisely 250 kHz. A calcite beam splitter separates the two beams laterally, then a half-wave plate rotates the polarization of one beam to make it parallel to the polarization of the other beam so that the two beams can subsequently be made to interfere with each other.

An assembly of beam splitters and lenses directs the beams onto the specimen surface at two spots. The distance [1 in. (2.54 cm)] between the spots constitutes the gauge length for measuring strain. At each spot, the beams are incident from opposing angles ($+\phi$ and $-\phi$) relative to the perpendicular to the surface, and thus form interference fringes on the surface. The distance (d) along the surface between successive fringes is given by $d = \lambda/2\sin\phi$, where λ is the wavelength of the laser beams. Light from the interference fringes in each spot is reflected to a photodetector in the optical head that contains the beam splitters and lenses; the inherent partial diffuse reflectivity of almost any specimen surface results in scattering of sufficient light for measurement by the photodetectors.

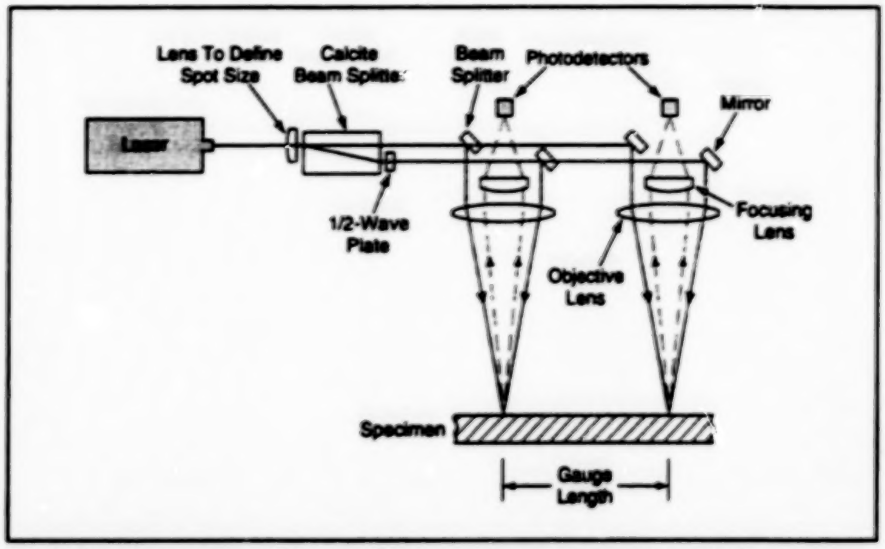

The Optical Components of the Laser Extensometer are arranged to provide for noncontact, interferometric measurement of strain in the specimen. The instrument is sensitive to strain along the line between the illuminated spots, and is insensitive to rigid-body motion of the specimen.

The temporal variation of difference between the phases of the two beams causes the interference fringes to move along the surface so that at each spot, the brightness fluctuates and the fluctuations can be measured in the output of the corresponding photodetector. When the surface remains fixed relative to each spot, the output of each photodetector includes a sinusoidal component that varies with time at the beat frequency of 250 kHz, and the difference between the phases of these components of the outputs of the two photodetectors remains constant.

When the reflective particles on the surface move against or with the motion of the fringes with a speed v, the frequency increases or decreases, respectively, by an amount v/d, and the difference between the phases varies accordingly. The phase of each photodetector output is compared with a reference phase, obtained from a detector inside the laser, that is used to stabilize the laser difference frequency at 250 kHz. A digital phase meter tracks the resulting relative phases and the difference between them; this phase difference is a direct measure of the strain along the line between the illuminated spots on the specimen. Because of the differential nature of the difference between the relative phases, the effect of any rigid-body motion of the specimen is automatically canceled.

This capability of the laser extensometer has been demonstrated in measurements on a variety of surfaces at temperatures up to 1,000 °C. Measurements are updated at a sampling rate of 125 kHz, and the update rate for display of output data is 2.5 kHz. The instrument can resolve strains as small as 5×10^{-6}.

This work was done by David L. Carlson of Optra, Inc., and David W. Voorhes of Lytron, Inc., for **Lewis Research Center**. *Further information is contained in a TSP [see page 1].*

Inquiries concerning rights for the commercial use of this invention should be addressed to the Patent Counsel, Lewis Research Center [see page 1]. Refer to LEW-15538.

15

Deicing-Fluid and Ice-Thickness Monitor for Aircraft

The crew is alerted to the need for corrective action.

Ames Research Center, Moffett Field, California

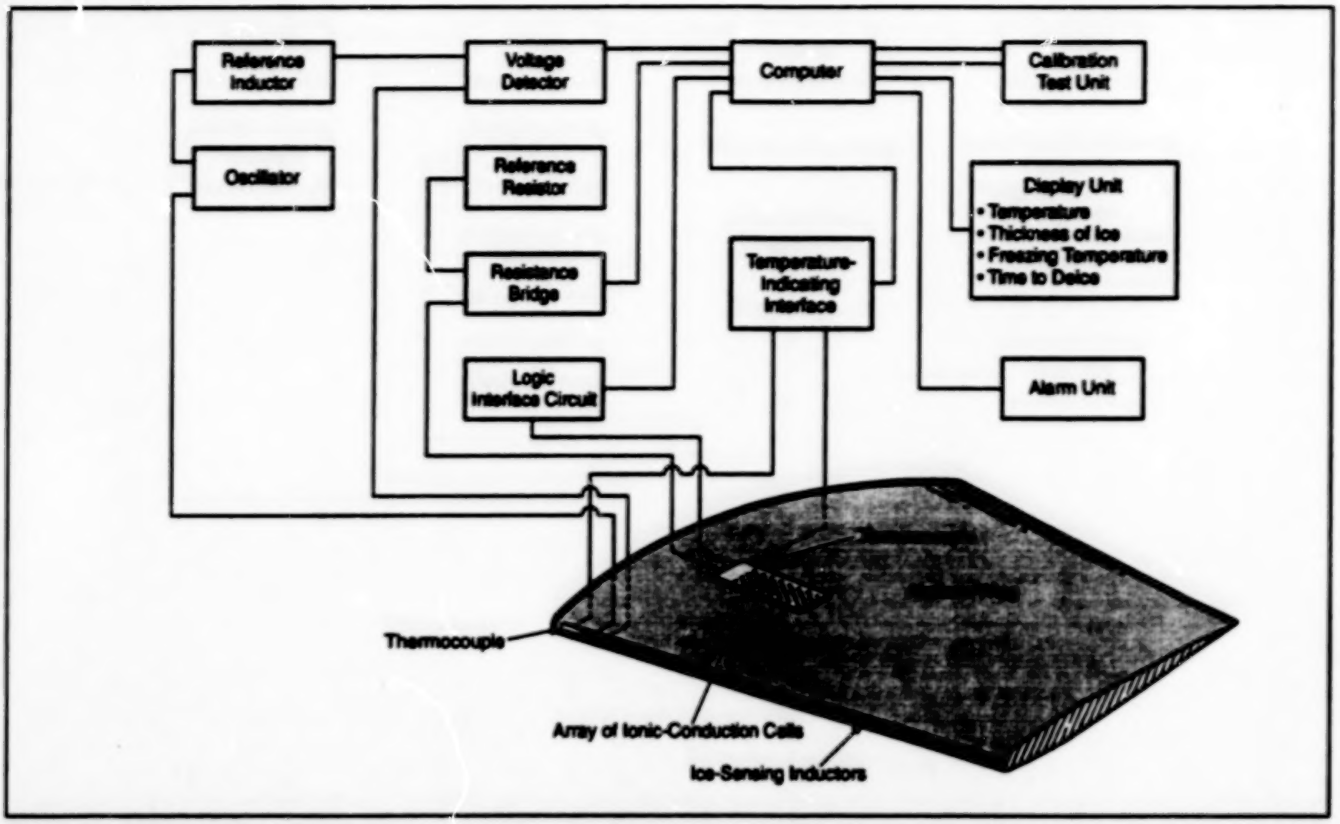

This Instrumentation System determines the ambient temperature, the thickness of ice (if any) in one area, and the freezing temperature of liquid (if any) in another area. The system also extrapolates the trend in the condition of the liquid to predict the time remaining until the liquid freezes.

An instrumentation system measures the thickness of ice and provides information on the effectiveness of deicing fluid on critical surfaces of an aircraft. By providing an early indication of the accretion of ice during flight, the system enables the crew of the aircraft to make a timely correction (e.g., changing course and/or altitude) before the ice becomes dangerously thick. When the aircraft is on the ground, the system can be used to determine whether there is a need to spray deicing fluid on the wings and other critical surfaces; thus, the system provides guidance to ensure that the amount of deicing fluid used is sufficient to ensure safety but is no more than that, thereby helping to minimize pollution of the airport environment from excess deicing fluid.

The system (see figure) includes ice-sensing inductors and a thermocouple embedded in a thin layer of dielectric material on a critical aircraft surface, a thin array of ionic-conduction cells and another thermocouple mounted on another critical aircraft surface (or on a different part of the same surface), and an assembly of analog and digital electronic circuits. The ice-sensing inductors comprise a transmitting and a receiving inductor; in effect, primary and secondary transformer windings. The transmitting inductor is excited by an oscillator at an audio or radio frequency chosen so as not to interfere with other electronic equipment in the aircraft. The coefficient of coupling between the two inductors, and thus the output voltage of the receiving inductor, depends on the thickness of overlying ice. Accordingly, the output of the receiving inductor is processed via a voltage detector and a computer, wherein it is compared with a reference voltage to determine the thickness of ice. The reference voltage for this purpose is determined during operation in a calibration mode, in which the excitation is supplied to a reference inductor instead of the ice-sensing inductors. The temperature reading provided by the thermocouple mounted with the ice-sensing inductors constitutes additional information that the computer uses to determine whether the measurement indicates the thickness of ice or indicates something else.

The array of ionic-conduction cells provides measurements of the surface electrical conductivity, which is an indication of the ionic conductivity and thus the concentration of deicing fluid in the surface film of liquid that remains after deicing fluid has been sprayed on and the excess has dripped off. By use of a logic interface circuit operating under computer control, the cells in the array can be activated one at a time and interrogated via a resistance bridge to obtain spatially resolved data on the concentration of deicing fluid. During operation in the calibration mode, the resistance bridge is connected to a reference resistor instead of one of the ionic-conduction cells.

The concentration of deicing fluid in the surface film of liquid decreases as the film becomes diluted with liquid water from fog, rain, snow, and/or melting ice. The freezing temperature of the film increases with decreasing concentration in a known way; thus, the computer is programmed to calculate the present freezing temperature of the surface film of liquid from the concentration as determined from the conductivity measurements. The computer compares this freezing temperature with the

actual ambient temperature measured by the thermocouple mounted with the ionic-conductivity cells. It also extrapolates the trend of recent conductivity measurements to predict when the freezing temperature will reach the actual ambient temperature. The predicted time thus serves as a deadline to spray on more deicing fluid or take other corrective action.

This work was done by H. Lee Seegmiller of **Ames Research Center.** *Further information is contained in a TSP [see page 1].*

This invention has been patented by NASA (U.S. Patent No. 5,523,959). Inquiries concerning nonexclusive or exclusive license for its commercial development should be addressed to the Patent Counsel, Ames Research Center [see page 1]. Refer to ARC-12045.

Air-Sampling System Measures Dew Point in a Wind Tunnel

This system gives accurate readings in real time.

Lewis Research Center, Cleveland, Ohio

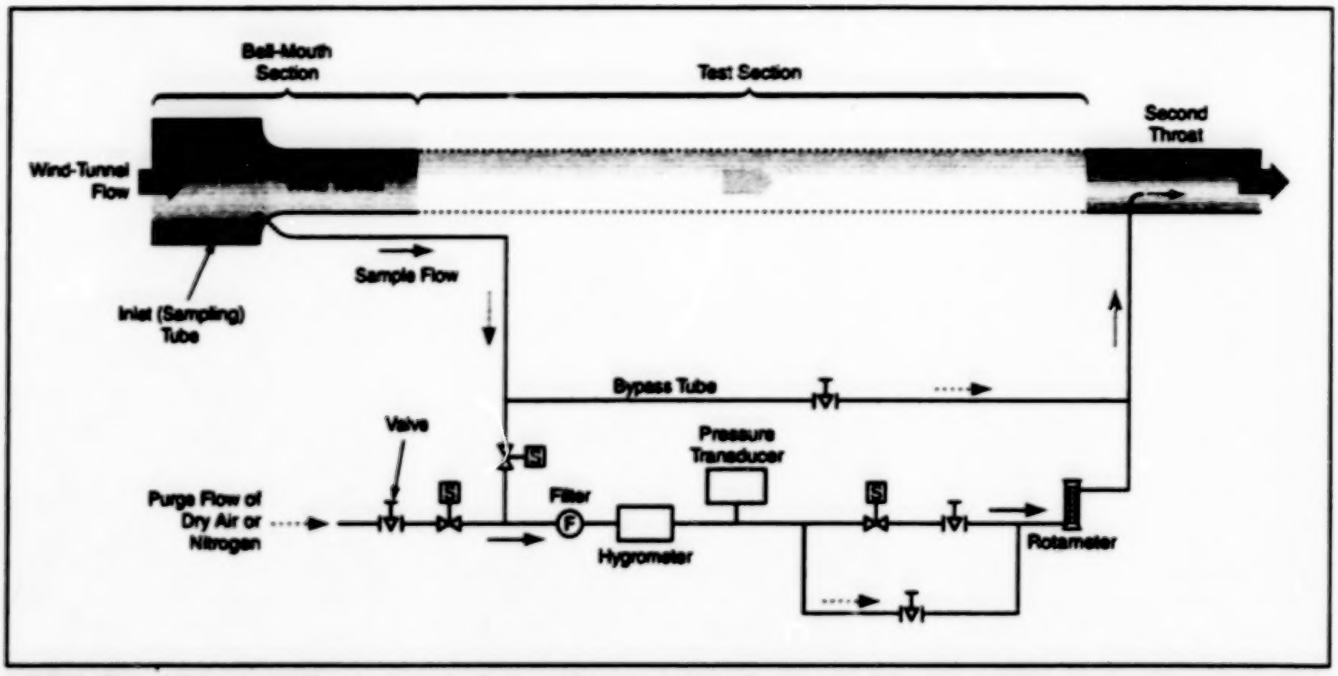

A Sample Flow of Air is extracted from a supersonic wind tunnel for measurement of its dew point. This system operates over the entire pressure range of the wind tunnel [2 to 45 psia (absolute pressure of 14 to 310 kPa)]. There is no need for a vacuum pump to provide the sample flow because this flow is driven by the pressure drop along the test section of the wind tunnel.

An improved instrumentation system measures the dew point of air flowing in a supersonic wind tunnel. This system was developed to replace a trouble-prone instrument that had to be operated manually in a trial-and-error procedure. Because the procedure took several minutes to acquire each reading, the readings could not be relied upon to keep up with changing flow conditions, and the cost of tunnel drive power expended unproductively quickly mounted. Other instruments that were tested in an effort to replace that instrument have exhibited various combinations of slow response, erratic readings, and high susceptibility to contamination. In contrast, the present system has been found to constitute a high-response, accurate, dependable instrument that provides nearly-real-time dew-point readings under wind-tunnel operating conditions.

The main sensory component of the present system is a commercial hygrometer with a proprietary moisture detector built on a small silicon chip and with closed-loop temperature control that compensates for the effect of ambient temperature from –40 to +113 °F (–40 to +45 °C). The hygrometer operates satisfactorily at flow rates from 50 to 1,500 cm³/min or in static conditions at pressures from 0 to 4,000 psig (gauge pressures from 0 to 28 MPa). The hygrometer responds to a step change in moisture in less than 1 minute, with a sensitivity characterized by a change in dew point of 0.002 °F (=0.001 °C). The range of the hygrometer is –76 °F to +32 °F (–60 to 0 °C) with an accuracy of ±3 °C.

The hygrometer is installed in a wind-tunnel air-sampling system, as indicated schematically in the figure. A pressure transducer is located immediately downstream of the hygrometer. The rate of flow through the hygrometer is monitored by use of a rotameter. A bypass tube makes it possible to increase the sample flow without incurring excessive flow through the hygrometer.

Before the wind tunnel begins to operate, the sampling system and hygrometer are purged with dry air or nitrogen. Once the wind-tunnel compressor has reached operating speed and an air dryer that is part of the wind-tunnel equipment has begun to function, solenoid valves are actuated to (1) switch off the purge flow, (2) connect the upstream end of the hygrometer plumbing to an inlet tube that samples the air in a bell-mouth section upstream from the test section of the wind tunnel, and (3) connect the downstream end of the hygrometer plumbing to an outlet tube that ends in a rearward-facing port at a point downstream inside the wind tunnel downstream of the test section. Thus, the sampling system utilizes the pressure drop along the test section to obtain the sample flow.

The instrumentation system includes an in situ calibration system (omitted from the figure for the sake of clarity) built around a commercial dew-point generator that provides a wide range of stable dew-point conditions. The calibration dew points are measured by use of a chilled-mirror hygrometer, which serves as a transfer standard provided by a calibration laboratory.

This work was done by Philip Z. Blumenthal of NYMA, Inc., for **Lewis Research Center**. *Further information is contained in a TSP [see page 1].*

Inquiries concerning rights for the commercial use of this invention should be addressed to NASA Lewis Research Center, Commercial Technology Office, Attn: Tech Brief Patent Status, Mail Stop 7–3, 21000 Brookpark Road, Cleveland, Ohio 44135. Refer to LEW-16443.

Parallel-Processing Program for Assimilation of Weather Data

Observations can be used to refine forecasts in real time.

NASA's Jet Propulsion Laboratory, Pasadena, California

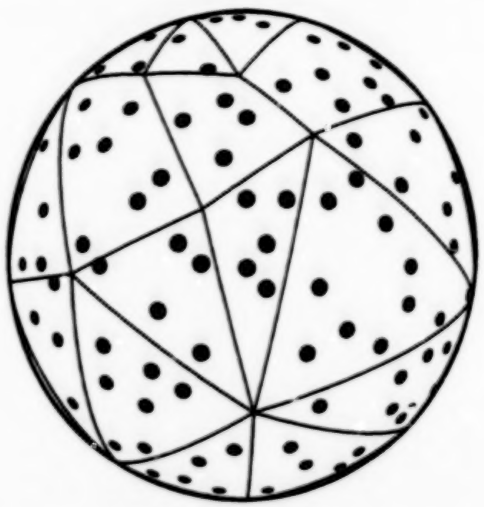

REGIONS CONTAINING OBSERVATION POINTS

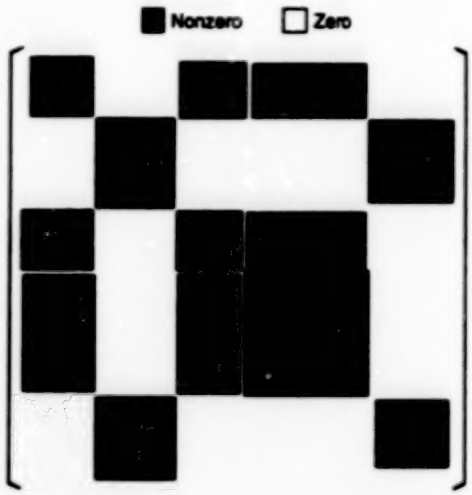

CORRELATION MATRIX WITH BLOCK STRUCTURE

The Surface of the Earth Is Partitioned into regions that contain approximately equal numbers of observation points. Correlations in regions centered more than 6,000 km apart are set to zero, resulting in a matrix with a block structure.

The parallel Physical-space Statistical Analysis System (PSAS) computer program was developed to exploit parallel processing on hundreds or even thousands of computer nodes to assimilate weather data more than 100 times as fast as on a conventional supercomputer, such as a Cray C90 (or equivalent). For example, the assimilation of data from a set of 80,000 observations at various locations around the Earth takes about 5 hours of central-processing-unit time on a single-head Cray C90 (or equivalent) computer, estimated by the Data Assimilation Office at Goddard Space Flight Center, who first developed the C90 version of the PSAS program. By use of parallel PSAS in a 512-node Paragon (or equivalent) computer, the same data can be assimilated in a total time of only 158 seconds; this includes time spent reading data from and writing data onto magnetic disks. Thus, the performance of parallel PSAS greatly exceeds the requirement for assimilation of weather data in real time in the sense that the total processing time for assimilation is much less than the 6-hour standard interval between meteorological observations. Indeed, the speed achievable with PSAS is great enough to enable more than 100 assimilations per day, making it practical to reevaluate weather data from past years.

"Assimilation" as used here denotes a fusion of (1) data from observations at a given time with (2) forecast data for the same time produced by another computer program. A typical forecast program produces data on a regular grid with intervals of 2° in latitude, 2.5° in longitude, and between 14 and 22 altitudes. The observational data are obtained from many sources, some of which (e.g., weather balloons) are moving from this six-hour interval to the next six-hour interval, and most or all of which may not be located at regular grid points. In the assimilation process, (1) the forecast data are interpolated from the regular grid to the observation points, (2) the observational data are combined with the forecast data through a statistical process similar to that of a Kalman filter to obtain an optimal estimate of the state of the weather system, and (3) the optimal estimate is interpolated from the observation locations back onto the regular grid.

The computation-intensive part of the assimilation process is the solution of a system of linear equations in N unknowns, where N is typically as large as 10^5. The challenge posed by the assimilation problem lies in the size of the $N \times N$ matrix of this system of equations. To store the entire matrix, one would need 10GB (in single precision) or 20GB (in double precision) of memory, exceeding the capacity of any currently available sequential computer. However, this requirement does not exceed the total distributed memory (16GB) of the 512-node parallel processor. Moreover, the huge number of floating-point computations for solving the equations can be distributed to individual nodes, reducing the solution time dramatically.

The problem then becomes one of how to distribute parts of the matrix to the nodes.

In an approximation based on a cutoff in correlations of observations made more than 6,000 km apart on the surface of the Earth, 74 percent of the matrix elements can be set to zero. This approximation can be utilized and modified in such a way as to impose a structure on the matrix. By use of a concurrent partitioning algorithm that adapts readily to different sets of observations, the surface of the Earth is divided into regions that contain approximately equal numbers of observations. The correlation cutoff is then enforced at the region level (see figure); that is, all observations in one region are treated as either correlated to all observations in another region or else not correlated to any observations in the other region, depending on whether the centers of the two regions are closer or farther than 6,000 km. This modified version of the correlation cutoff partitions the matrix into a block structure, in which the elements in 74 percent of the blocks are zero.

This modification leads to a correct and consistent approximate solution that differs from the solution for the nonregionalized version by a root-mean-square error of 1 to 2 percent. The big advantage gained from the block pattern is the ability to use a highly efficient matrix-vector multiplication routine that is designed for block matrices and that is an order of magnitude faster than are conventional techniques designed for sparse matrices.

This work was done by Hong Q. Ding and Robert D. Ferraro of Caltech for **NASA's Jet Propulsion Laboratory**. *Further information is contained in a TSP* *[see page 1]*.

NPO-19936

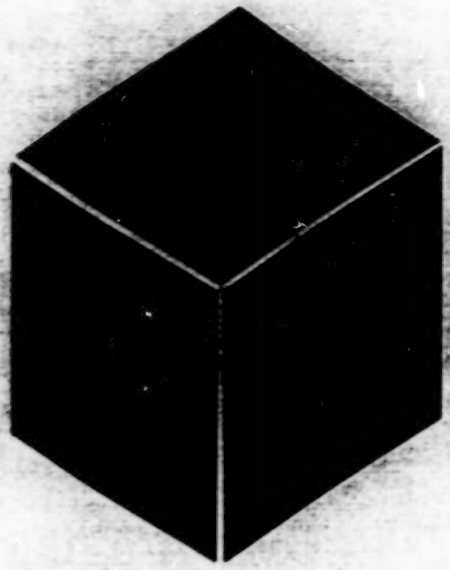

Materials

Hardware, Techniques, and Processes

29 Covalent Cross-Linking for Strengthening Composite Materials
30 Polymeric Electrolyte Membrane Materials for Fuel Cells

Covalent Cross-Linking for Strengthening Composite Materials

Fiber molecules would be covalently bonded to matrix molecules.

Lewis Research Center, Cleveland, Ohio

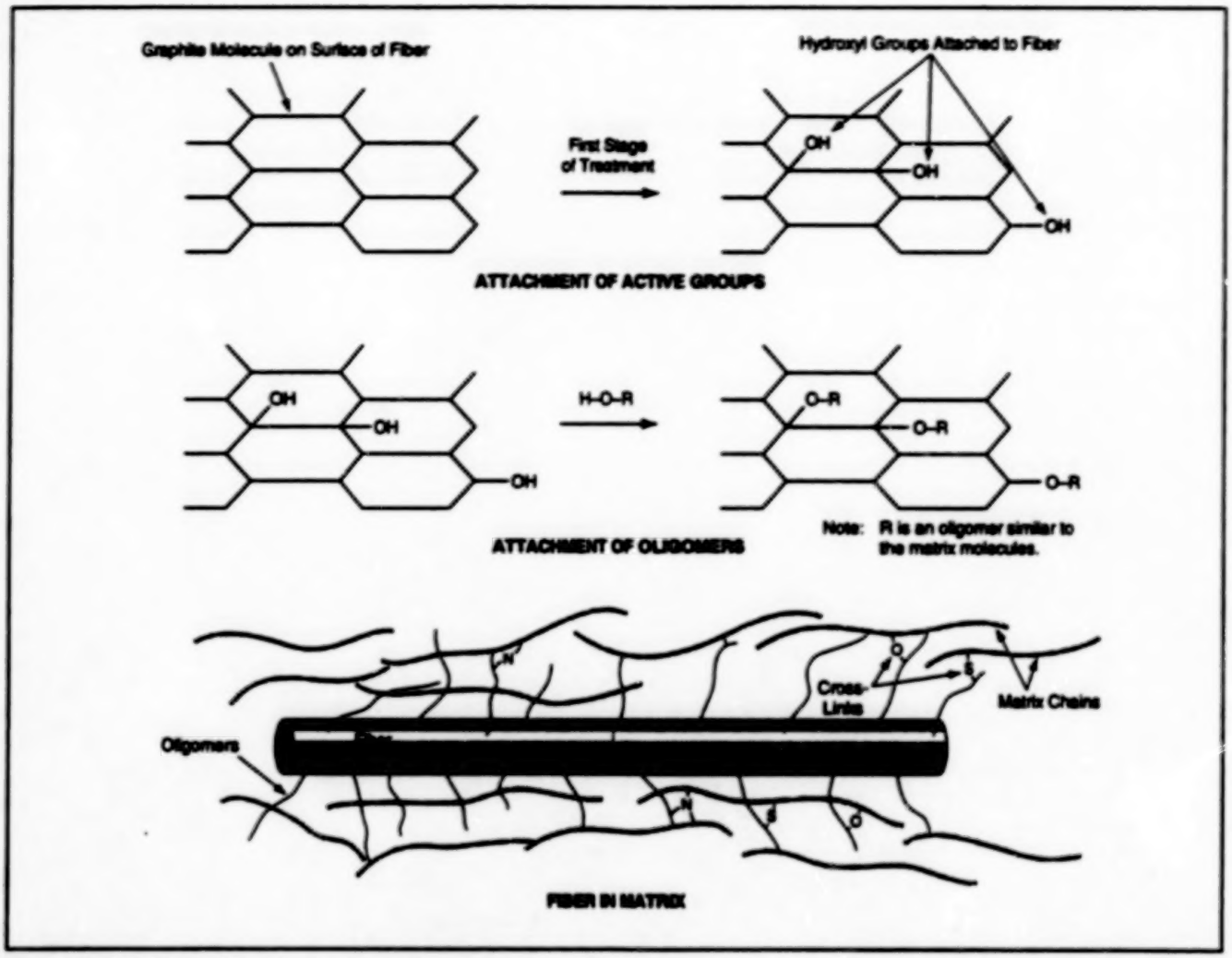

Fibers Would Be Made "Hairy" by chemical attachment of oligomers. The oligomers would form covalent bonds and/or would tangle with matrix molecules, with resultant strengthening of matrix/fiber bonds.

In a proposed method of strengthening matrix/fiber composite materials, surfaces of fibers would be chemically treated to provide some covalent bonds between fiber and matrix molecules. The method was conceived in an effort to strengthen bonds between carbon fibers and rubber matrices in tires, but should also be applicable to fibers made of other materials and to various polymeric matrix materials.

The figure illustrates the basic principles of the method as applied to carbon (in particular, graphite) fibers in a polymeric matrix. In preparation for chemically treating the fibers and incorporating them into the matrix, one would choose a chemically active group capable of attachment to at least two sites — one on the graphite surface of the fiber and one on an oligomer to be added subsequently. Examples of groups that would be suitable for this purpose include hydroxyl (–OH), amino ($–NH_2$), cyano (–CN), and thiol (–SH). The chosen groups would be attached to the fiber in the first stage of treatment. For example, hydroxyl groups could be attached by one or more of several oxidation treatments that could include the use of nitric, sulfuric, or perchloric acid; superheated steam; heating in air; plasma ashing; and/or beams of oxygen ions. The number of groups attached could be controlled, by adjusting treatment conditions, to optimize the fiber/matrix bond to be formed subsequently.

In the second stage of treatment, oligomers similar to the matrix molecules (e.g., isoprenoids in the case of a rubber matrix) would be attached to the outer ends of the groups that had been attached to the fibers in the first stage of treatment. This could be done by addition of oligomers that form ester or ether linkages in the case of hydroxyl groups (or that form analogous linkages with whichever of the other groups is chosen). The resulting bonds between the oligomers and the fibers must be strong enough to withstand subsequent processing steps. The oligomers could be chosen to have lengths that are optimum for the desired matrix/fiber bonds. In effect, the fibers as treated thus far would have been made "hairy" by the attachment of oligomeric units.

In the third stage of treatment, the matrix precursor material would be introduced, and the resulting composite would be cured. As cross-links formed between matrix molecules during the curing proc-

ess, some cross-links would also form between matrix molecules and the matrix-like oligomers attached to the fibers. Thus the oligomers and fibers would become covalently bonded to the matrix. Even if the matrix material were one that does not form covalent cross-links, matrix/fiber bonds could still be strengthened by use of long oligomers that would mix and tangle with molecular chains of the matrix.

This work was done by James R. Gaier of **Lewis Research Center**. *Further information is contained in a TSP [see page 1].*

Inquiries concerning rights for the commercial use of this invention should be addressed to the Patent Counsel, Lewis Research Center [see page 1]. Refer to LEW-16244.

Polymeric Electrolyte Membrane Materials for Fuel Cells

Advantages include low cost, thermal stability, low methanol permeability, and high proton conductivity.

NASA's Jet Propulsion Laboratory, Pasadena, California

A class of improved proton-conductive sulfonic acid polymeric membranes has been developed for use as solid electrolytes in hydrogen/oxygen and direct methanol fuel cells. These membrane materials are denoted generally as highly sulfonated poly(ether ether ketone) (H-SPEEK). In comparison with previously developed commercial fuel-cell membrane materials, H-SPEEK is more stable in the optimum range of operating temperatures (100 to 200 °C), is less permeable by methanol, and costs less.

In an experiment on the preparation of H-SPEEK, 120 g of PEEK (grade 450p) was stirred in 1,200 mL of sulfuric acid at room temperature for 4.5 hours. The resulting homogeneous solution was heated to 91 °C for 1 hour. The reaction in the solution (see Figure 1) was then quenched and the solution cooled to room temperature. Once precipitated from the solution, the polymer was washed to remove excess acid. At an approximate pH of 5, samples of the polymer were dried under ambient conditions for various times from 36 to 72 hours. As thus prepared, H-SPEEK exhibited an equivalent molecular weight of 365 daltons. Unlike poly(ether ether ketone) (PEEK), H-SPEEK is soluble in aqueous organic solvents.

Once the H-SPEEK was dry, a 30-g sample was dissolved in an acetone/water solution. To this solution, approximately 3 g of glycerine was added, and the resulting mixture was filtered over a celite pack. From the filtered mixture, films were cast in low-thermal-expansion glass dishes, evaporation times ranging from 24 to 48 hours. The cast films had lateral dimensions of 6 by 8 in. (15 by 20 cm) and thicknesses ranging from 3 to 20 μm.

After the films were set, the dishes were heated to a temperature of 120 °C under vacuum to promote cross-linking (see Figure 2). The amount of cross-linking in each film was determined by the heating time. After the cross-linked films were removed from the dishes, they were conditioned in boiling water (to ensure the stability of the resulting membranes at high temperatures) and soaked to remove excess glycerine.

The equivalent molecular weight of one of the H-SPEEK films thus treated was found to be 504 daltons. Nuclear-magnetic-resonance analysis of this film prior to cross-linking indicated that there was one sulfonic acid group per molecular repeat unit. Back-titration of a series of solutions containing samples of this film taken after cross-linking indicated that 28 percent

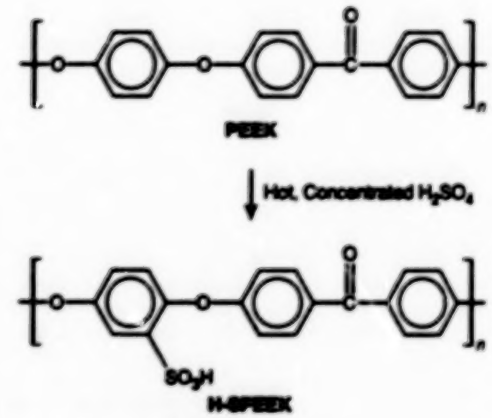

Figure 1. PEEK Is Sulfonated in hot, concentrated sulfuric acid to make H-SPEEK.

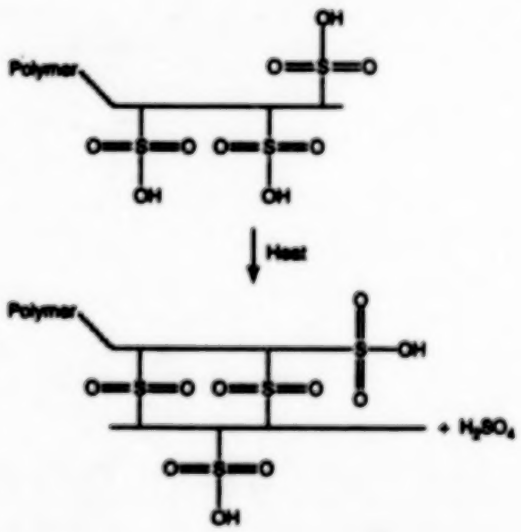

Figure 2. H-SPEEK Can Be Cross-Linked by heating, with conversion of sulfonic acid groups to sulfone groups. Cross-linking can impart desirable properties — notably, reduction of permeability by methanol.

its sulfonic acid groups had been converted to sulfone groups by the cross-linking process.

H-SPEEK is soluble in such organic solvents and solvent mixtures as dimethyl formamide, dimethyl acetamide, n-methyl pyrrolidinone, dimethyl sulfoxide, and water/acetone. Prior to cross-linking, it is also soluble in water/methanol. Solutions of H-SPEEK in such solvents can be used to make proton-conductive binders in the fabrication of electrodes for fuel cells.

Membranes made from H-SPEEK have been found to be comparable to a commercial membrane with respect to mechanical strength and proton conductivity (the magnitude of which is determined by the degree of sulfonation). Cross-linking in H-SPEEK can be achieved without significant loss of proton conductivity. Accordingly, a combination of cross-linking within the membrane and modification of the surface of the membrane can be used to reduce the undesired permeability of an H-SPEEK membrane by methanol without greatly reducing the desired permeability of the membrane by protons.

This work was done by Shaio-Ping S. Yen, Eva Graham, Sekharipuram R. Narayanan, Andre Yavrouian, and Gerald Halpert of Caltech for **NASA's Jet Propulsion Laboratory**. *Further information is contained in a TSP [see page 1].*

In accordance with Public Law 96-517, the contractor has elected to retain title to this invention. Inquiries concerning rights for its commercial use should be addressed to

Larry Gilbert, Director
Technology Transfer
California Institute of Technology
Mail Code 315 - 6
Pasadena, CA 91125
(818) 395-3288

Refer to NPO-19541, volume and number of this NASA Tech Briefs *issue, and the page number.*

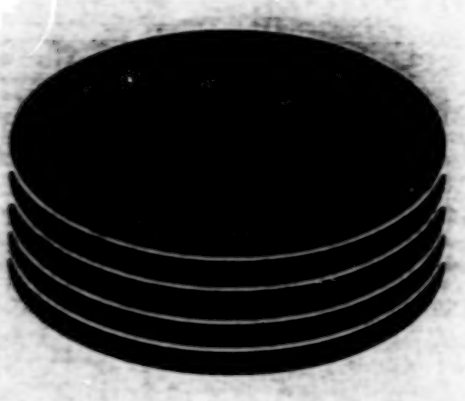

Computer Programs

Electronic Systems

35 Software Generates Commands for Operating Remote Instruments
35 Designing a Spacecraft Data-Communication System
35 Scheduling Software for a Network of Communication Antennas

Physical Sciences

35 Software for Processing SAR Data From the Magellan Project

Mathematics and Information Sciences

36 Prototype System for Development of Scheduling Software
36 Telemetry Management Flight Software
36 Software for On-Board Planning in a Nearly Autonomous System

Computer Programs

These programs may be obtained from COSMIC. Please contact

COSMIC®
Computer Services Annex
University of Georgia
Athens, GA 30602
Telephone No. (404) 542-3265.

Electronic Systems

Software Generates Commands for Operating Remote Instruments

The DATA-CHASER Automated Planner/Scheduler (DCAPS) computer program automatically generates sequences of low-level commands for remote control of equipment to achieve high-level goals defined by users. DCAPS is designed specifically for controlling the DATA-CHASER, which is a package of spectral imaging instruments to be flown aboard the space shuttle to observe the Sun. DCAPS utilizes artificial-intelligence techniques and a scheduling algorithm of the iterative repair type (algorithms of this type have been used in commercial operations). Like other iterative repair algorithms, this one iteratively and selectively resolves conflicts within the applicable constraints on time and resources. The DCAPS version of this algorithm is adapted specifically to the DCAPS commanding application. DCAPS provides for a natural representation of problems that arise in this application and for interaction with users, enabling them to become directly involved in the sequencing of commands. DCAPS provides for simple (from the users' perspective), nondisruptive rescheduling following any changes in the state of the spacecraft or in goals defined by the users.

This program was written by Steve Chien, Gregg Rabideau, Tobias Mann, and Peter Stone of Caltech for **NASA's Jet Propulsion Laboratory**. *Further information is contained in a TSP [see page 1].*

This software is available for commercial licensing. Please contact Don Hart of the California Institute of Technology at (818) 393-3425. Refer to NPO-20085.

Designing a Spacecraft Data-Communication System

A computer program gives preliminary estimates that are useful for designing the spacecraft end of a radio-communication link for transmitting digital data from low orbit around the Earth to a ground station. [It is related to another program described in "Computing Supportable Bit Rates in Radio Communications" (NPO-20039), *NASA Tech Briefs*, Vol. 21, No. 5 (May 1997), page 50.] The major overall functions of this program are to generate a link budget quickly (a systematic table of gains and losses of the link) and to give approximate values of parameters of a design to satisfy the data-communication requirements. Like the program described in the cited prior article, this program is based partly on established equations for relationships among radiated power, various link margins, gains, losses, modulation index, data rate, distance, antenna dimensions, frequency, receiver noise temperature, and other relevant parameters. Additional factors that are taken into account in this program are the duration of visibility of the spacecraft from the ground station for the orbit in question, the time taken by the ground station to acquire the spacecraft carrier signal, and whether the spacecraft antenna is aimed toward the ground station or toward the nadir. Like the other program, this program is written in the Excel 5.0 software system.

This program was written by Anil Kantak and Faiza Lansing of Caltech for **NASA's Jet Propulsion Laboratory**. *Further information is contained in a TSP [see page 1].*
NPO-19997

Scheduling Software for a Network of Communication Antennas

The Demand Access Network Scheduler (DANS) computer program automatically schedules and allocates resources for a network of ground-station communication antennas — specifically, the Deep Space Network. DANS was developed because the manual scheduling and rescheduling of large numbers of tracks for ground stations is a costly, labor-intensive, and knowledge-intensive task that makes an excessive demand on scarce personnel resources. DANS starts from a baseline schedule, then uses priority-driven, best-first, constraint-based search and iterative optimization techniques to perform priority-based rescheduling in response to changes in tracking requests, malfunctions in equipment, or inclement weather. DANS performs a local search to find good rescheduling solutions quickly while minimizing disruptions associated with changes in the baseline schedule. DANS first considers the antenna-allocation process, inasmuch as antennas are the central focus of contention for resources. After establishing a range of antenna options, DANS considers the allocation of 5 to 13 subsystems per track (out of the tens of shared subsystems at each antenna complex).

This work was done by Steve Chien, Ray Lam, and Quoc Vu of Caltech for **NASA's Jet Propulsion Laboratory**. *Further information is contained in a TSP [see page 1].*

This software is available for commercial licensing. Please contact Don Hart of the California Institute of Technology at (818) 393-3425. Refer to NPO-20084.

Physical Sciences

Software for Processing SAR Data From the Magellan Project

This software is superior to previous Magellan software that performed similar functions.

MGN USP is a computer program for utilizing synthetic-aperture-radar (SAR) data from the Magellan project, which explored the hidden surface of the cloud-covered planet Venus. The "USP" part of the name of this program signifies "UNIX-based SAR Processor." The major functions of the program are reading the experimental data record (EDR) from tape or disk, processing the raw data, and converting them to image data in a format called "Full-Resolution Basic Image Data Record" (F-BIDR).

MGN USP is superior to a previous Magellan-SAR-data-processing program in that it achieves higher precision

in the areas of range-migration compensation, Doppler compensation, azimuth-interpolation Kaiser weights, radiometric compensation, and geometric rectification. MGN USP also features provisions for an improved multilook overlay.

MGN USP is written in FORTRAN 77 and C language for a SunOS or Solaris computer workstation (SPARCserver 10, SPARC 670MP, or SPARC 690MP) with 128MB of memory, 1.3GB of disk space, and a nine-track tape drive or an 8-mm tape drive with SCSI interface. The standard distribution medium for MGN USP is one 4-mm DAT in UNIX tar format. MGN USP is also available on 8-mm or nine-track tape by request. MGN USP was released to COSMIC in 1994 and is a copyrighted work with all copyright vested in NASA.

This program was written by M. Jin, L. Chen, and A. Chu of Caltech for **NASA's Jet Propulsion Laboratory**. *Further information is contained in a TSP [see page 1].*
NPO-19501

Mathematics and Information Sciences

Prototype System for Development of Scheduling Software

The Automated Scheduling and Planning Environment (ASPEN) computer program is a prototype system for developing application programs for automated scheduling. ASPEN is an object-oriented system that contains a modular, reconfigurable, reusable set of software components that implements the elements commonly found in complex automated-scheduling applications. The components include the following:

- An expressive constraint-modeling language that enables the user to naturally define the application domain,
- A constraint-management system for representing and satisfying activity requirements while not violating constraints,
- A temporal-reasoning system for expressing and maintaining temporal constraints,
- A set of search algorithms for generating and repairing schedules, and
- A graphical interface to help the user visualize and modify plans and schedules.

These components can work together to provide either a fully autonomous command-planning-and-scheduling system, or a mixed-initiative system in which the problem-solving process is interactive. ASPEN is written in C++ using the STL and Lecia libraries and the X-Windows environment.

One of the key features of ASPEN is the ability to repair a generated schedule using a search algorithm such as the "iterative repair" technique. Basically, the algorithm iteratively selects a schedule conflict and performs modifications in an attempt to resolve the conflict. The search algorithm automates decisions on what to repair and how to make the repair until all conflicts have been resolved. The iterative repair work builds on the previous NASA Tech Brief, "Software Generates Commands for Operating Remote Instruments," NPO-20085, in this issue.

ASPEN is currently being utilized in the development of an automated planner/scheduler for commanding a naval communications satellite and the New Millennium Program's first Earth-orbiting spacecraft (EO-1) as well as a scheduler for ground maintenance for Highly Reusable Space Transportation (HRST). By automating the command sequence generation process and by encapsulating the operation-specific knowledge, spacecraft commanding can be done by nonoperations personnel, hence allowing significant reductions in mission operations workforce with the eventual goal of allowing direct user commanding (e.g., commanding by scientists).

This program was written by Alex Fukunaga, Gregg Rabideau, Steve Chien, David Yan, Robert Sherwood, and Quoc Vu of Caltech for **NASA's Jet Propulsion Laboratory**. *Further information is contained in a TSP [see page 1].*

This software is available for commercial licensing. Please contact Don Hart of the California Institute of Technology at (818) 393-3425. Refer to NPO-20074.

Telemetry Management Flight Software

Telemetry Management Flight Software is a computer program designed originally for use in spacecraft, but could also be used in aircraft, balloon-borne instrument packages, or other telemetric instrumentation systems. This program manages telemetric data aboard a spacecraft in a highly configurable fashion. It provides a mission-independent (reusable) means of enabling spacecraft operators to make the most efficient use of low-bandwidth downlink telemetry channels, consistent with standards of the Consultative Committee for Space Data Systems (CCSDS). The program is flexible and makes the spacecraft telemetric system highly commandable. It automatically meters telemetry from multiple sources in a fair manner, on the basis of commanded priorities and bandwidth allocations. Features include automatic retransmission, ring-buffer management, and timed deletions. No other known software offers the particular combination of capabilities and reusability. This program runs under VxWorks on Motorola, MIPS, RAD6000, and other computers. It occupies about 100K of random-access memory.

This program was written by Scott Burleigh and Sanford M. Krasner of Caltech for **NASA's Jet Propulsion Laboratory**. *Further information is contained in a TSP [see page 1].*
NPO-19904

Software for On-Board Planning in a Nearly Autonomous System

The DS1 On-Board Planner and Scheduler (PS) software is a component of the artificial-intelligence system described in "A Remote Agent Prototype for Spacecraft Autonomy" (NPO-19992) *NASA Tech Briefs*, Vol. 21, No. 3 (March 1997), page 106. The artificial-intelligence system has been developed for use in small exploratory spacecraft and might also prove adaptable to other terrestrial robotic systems for which there is a need to implement nearly autonomous operation with only occasional high-level, possibly non-real-time human intervention. The PS software can reduce the cost and enhance the quality of a mission by (a) formulating detailed plans of action in response to high-level commands, (b) providing for robust responses to equipment failures to enable achievement of mission goals without human intervention, and (c) taking advantage of fortuitous events.

This program was written by Benjamin D. Smith, Steve A. Chien, David Yan, and Gregg Rabideau of Caltech; Nicola Muscettola of Recom Technologies; Chuck Fry, Kanna Rajan, and Sunil Mohan of Caelum Research; and Other Hansson of Thinkbank, Inc., for. This program was written by Caltech for **NASA's Jet Propulsion Laboratory**. *Further information is contained in a TSP [see page 1].*

This software is available for commercial licensing. Please contact Don Hart of the California Institute of Technology at (818) 393-3425. Refer to NPO-20063.

Mechanics

Hardware, Techniques, and Processes

39 Micromachined Planar Vibratory Microgyroscopes
40 Planar Vibratory Microgyroscope: Alternative Configuration
40 Modulation/Detection Technique for Measuring Acceleration
41 Micromachined Planar Vibratory Sensors With Mode Matching
42 Micromachined Silicon Vibratory Three-Axis Accelerometer

Micromachined Planar Vibratory Microgyroscopes

Improved designs promise to increase sensitivity and decrease drift and noise.

NASA's Jet Propulsion Laboratory, Pasadena, California

Micromachined planar vibratory microgyroscopes are undergoing development for use in monitoring the orientations of robots, scientific instruments, and other objects. A device of this type can be fabricated by use of silicon-on-glass or complementary metal oxide/semiconductor (CMOS) bulk-micromachining technology. Because they offer advantages of relatively small size, weight, and power consumption, vibratory microgyroscopes offer attractive alternatives to spinning-mass and optical gyroscopes in such applications.

Like other vibratory gyroscopes, a micromachined planar vibratory microgyroscope is based on a principle similar to that of the Foucault pendulum. First, a vibration is excited in one of two modes of the gyroscope structure. Then the Coriolis force associated with a rotation that one seeks to measure induces a transfer of energy from that vibrational mode to the other one. The vibration in the second mode is measured to obtain data from which the rotation can be inferred.

Vibratory microgyroscopes of older design are disadvantageous in several respects. They must be fabricated with extreme precision because their proper functioning depends on precise matching of mechanical resonances. Typical values of their vibrating masses are no greater than about 10^{-10} kg, typical values of their spring stiffnesses are no less than 1 N/m, and their resonance frequencies typically lie between 20 and 30 kHz. At such high resonance frequencies, the amplitudes of vibrations and thus the amplitudes of readouts are small, and consequently sensitivity is low. With such small masses, ratios of damping are large. The vibration actuators and vibration-sensing structures have small capacitances, and this also limits sensitivity. The net result of these disadvantageous characteristics is that drift rates can be as large as 5,000°/hour. The improved designs of the developmental micromachined planar vibratory microgyroscopes are intended to reduce drift rates to no more than 10°/hour.

A micromachined planar vibratory microgyroscope (see figure) includes four planar silicon plates connected together in a pattern resembling that of a clover leaf. The plates are suspended by four silicon slab springs. In the absence of input rotation, plates A and C are driven electrostatically out of phase to oscillate in seesaw mode in the z direction.

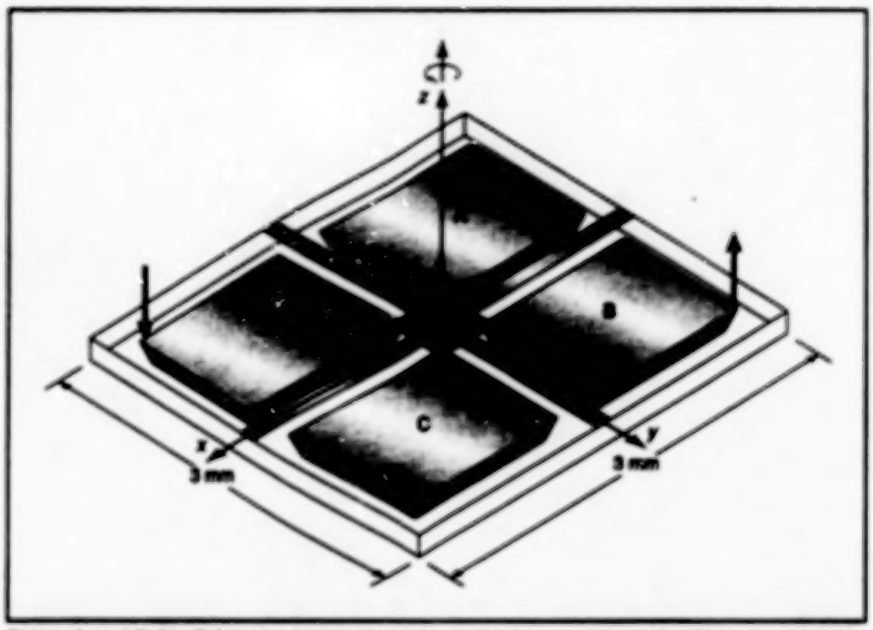

Plates A and D Are Driven to vibrate about the center in a seesaw mode. When the assembly rotates about the z axis, the Coriolis force couples some of the vibrational energy to the seesaw mode of plates B and D. The amplitude of the B-D seesaw mode is measured and used to infer the rate of rotation.

One seeks to measure rotation about the z axis. When such rotation occurs, the Coriolis force causes the plates B and D to also oscillate in a seesaw mode in the z direction; that is, the Coriolis force causes a transfer of energy from A-C seesaw mode to B-D seesaw mode. The displacements of plates B and D are detected by use of capacitive proximity sensors. These displacements are inversely proportional to the resonance frequency of the output (B-D seesaw) mode and proportional to (1) the amplitude of the input (A-C) displacement, (2) the rate of rotation about the z axis, and (3) the resonance quality factor, which is commonly denoted "Q" and is inversely proportional to the rate of damping.

In fabricating a micromachined planar vibratory microgyroscope, extreme precision for matching of resonances is not necessary. The symmetrical planar structure inherently matches the resonances of the input (A-C) and output (B-D) vibration modes. Typical vibrating-mass values for these devices range from 10^{-9} to 10^{-8} kg, typical spring stiffnesses are about the same as in older microgyroscopes (about 1 N/m or greater), and typical mechanical resonances lie approximately in the frequency range from 100 Hz to 1 kHz.

With these characteristics, micromachined planar vibratory microgyroscopes offer several advantages over older vibratory microgyroscopes: With lower resonance frequencies, outputs are larger. With larger masses, both thermal noise and rates of damping are reduced. The areas of driving and sensing structures are larger, resulting in larger capacitances and thus larger driving forces and larger output signals. Moreover, a micromachined planar vibratory microgyroscope can be driven off resonance, eliminating the need for mechanical matching between the input and output modes.

This work was done by William J. Kaiser, Tony K. Tang, and Randall K. Bartman of Caltech for NASA's Jet Propulsion Laboratory. Further information is contained in a TSP (see page 1).

In accordance with Public Law 96-517, the contractor has elected to retain title to this invention. Inquiries concerning rights for its commercial use should be addressed to

Larry Gilbert, Director
Technology Transfer
California Institute of Technology
Mail Code 315 - 6
Pasadena, CA 91125
(818) 395-3288

Refer to NPO-19713, volume and number of this NASA Tech Briefs issue, and the page number.

Planar Vibratory Microgyroscope: Alternative Configuration

A rod is attached at the center of the vibrating structure.

NASA's Jet Propulsion Laboratory, Pasadena, California

The figure illustrates a micromachined planar vibratory microgyroscope with a configuration like that described in the preceding article, except that a rod between 3 and 4 mm long and oriented along the *z* axis is attached rigidly to the center of the planar vibrating structure. This device offers the same advantages as do the micromachined planar vibratory microgyroscopes described in the preceding article, plus the additional advantage that the rod contributes to the moments of inertia about the *x* and *y* axes, thereby creating a more favorable inertia ratio. It also helps to place mechanical resonances in a desired low frequency range of 0.1 to 1 kHz.

The principle of operation is the same as that described in the preceding article, except that the rod plays an important part in the motion. As before, the purpose of the device is to measure rotation about the *z* axis. As before, four planar silicon plates are connected together in a pattern resembling that of a clover leaf, and the plates are suspended by four silicon slab springs; however, in this case, the rod is also attached to the central body where the springs and plates come together. As before, plates A and C are driven electrostatically to oscillate in a seesaw mode in the *z* direction. This seesaw motion causes the rod to engage in rotational oscillation about the *x* axis.

In the absence of rotation about the *z* axis, plates B and D remain stationary. When the device rotates about the *z* axis, the Coriolis force causes the rod to oscillate somewhat about the *y* axis, thereby causing plates B and D to also oscillate in a seesaw mode. Thus, when there is rotation about the *z* axis, the Coriolis force causes transfer of energy from the seesaw mode of plates A and C to the seesaw mode of plates B and D; the amplitude of oscillation in this mode is directly related to the rate of rotation about the *z* axis. This amplitude is measured capacitively to obtain a measure of the rate of rotation.

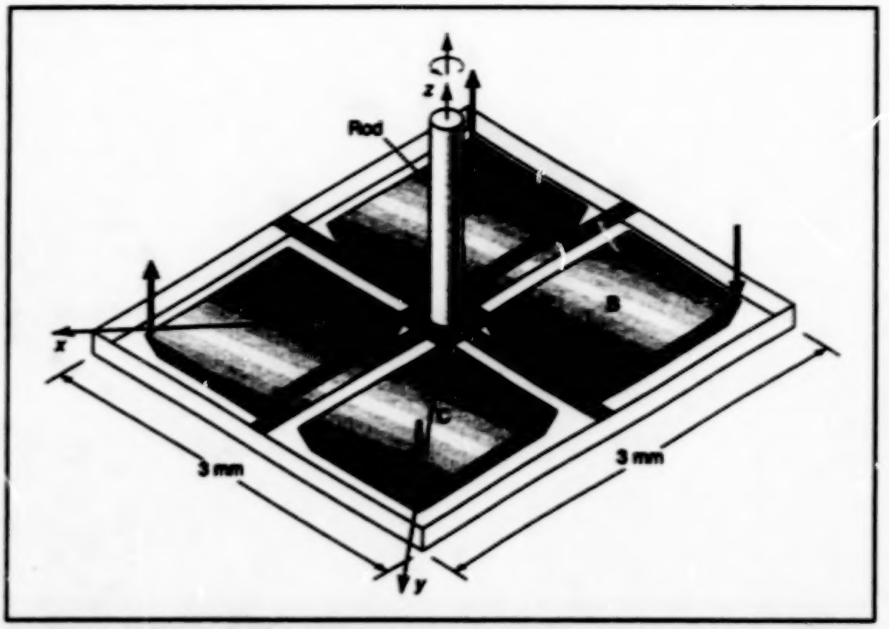

The Rod Contributes Additional Moment of Inertia about the *x* and *y* axes, thereby creating a more favorable inertia ratio and desirably lowering resonance frequencies. In other respects, this device is similar to the devices described in the preceding article.

This work was done by Tony K. Tang, William J. Kaiser, Randall K. Bartman, Jaroslave Z. Wilcox, Roman C. Gutierrez, Robert J. Calvet, and S. K. Tsang of Caltech for NASA's Jet Propulsion Laboratory. Further information is contained in a TSP [see page 1].

In accordance with Public Law 96-517, the contractor has elected to retain title to this invention. Inquiries concerning rights for its commercial use should be addressed to

Larry Gilbert, Director
Technology Transfer
California Institute of Technology
Mail Code 315 - 6
Pasadena, CA 91125
(818) 395-3288

Refer to NPO-19714, volume and number of this NASA Tech Briefs *issue, and the page number.*

Modulation/Detection Technique for Measuring Acceleration

Performances of accelerometers would be enhanced by lock-amplification of superimposed oscillations.

NASA's Jet Propulsion Laboratory, Pasadena, California

A proposed technique for increasing the signal-to-noise ratios of accelerometers is based on a concept of phase-sensitive detection and amplification of oscillations superimposed on the accelerations that one seeks to measure. The technique would be especially applicable to micromachined spring-and-proof-mass accelerometers and to conventional accelerometers mounted on suitably configured micromachined structures.

In a conventional spring-and-proof-mass accelerometer, the inertia of the proof mass causes the spring to deflect in a response to an acceleration along one axis. The resulting displacement of the proof mass can be measured by any of several well-known proximity-sensing techniques based, for example, on capacitance, piezoresistance, or quantum-mechanical tunneling of electrons. The acceleration can then readily be calculated from the measured displacement and the known stiffness and inertial properties of spring-and-proof-mass structure.

In an accelerometer designed to implement the proposed technique, the spring structure on which the proof

mass or conventional accelerometer would be mounted would include a spring substructure capable of deflection not only in the primary acceleration-sensing mode but also in a secondary vibration mode with a known resonance frequency and with displacements along the acceleration-sensing axis (see figure). By use of a suitable actuator driven at the resonance frequency, vibrations in this mode would be excited, thereby generating a resonance-frequency component of acceleration superimposed on the acceleration that one seeks to measure.

The use of phase-sensitive detection and amplification to increase signal-to-noise ratios is well known. The basic idea is to detect and amplify only the signal component at a specific known frequency and phase, thereby rejecting noise that occurs over a broad range of frequencies. In the proposed technique, phase-sensitive detection and amplification would be accomplished by processing the output of the displacement sensor through a lock-in amplifier that would be phase-locked to the oscillator used to excite the secondary vibrations.

This work was done by Tony K. Tang and Michael H. Hecht of Caltech for **NASA's Jet Propulsion Laboratory.** *No further documentation is available.*
NPO-20049

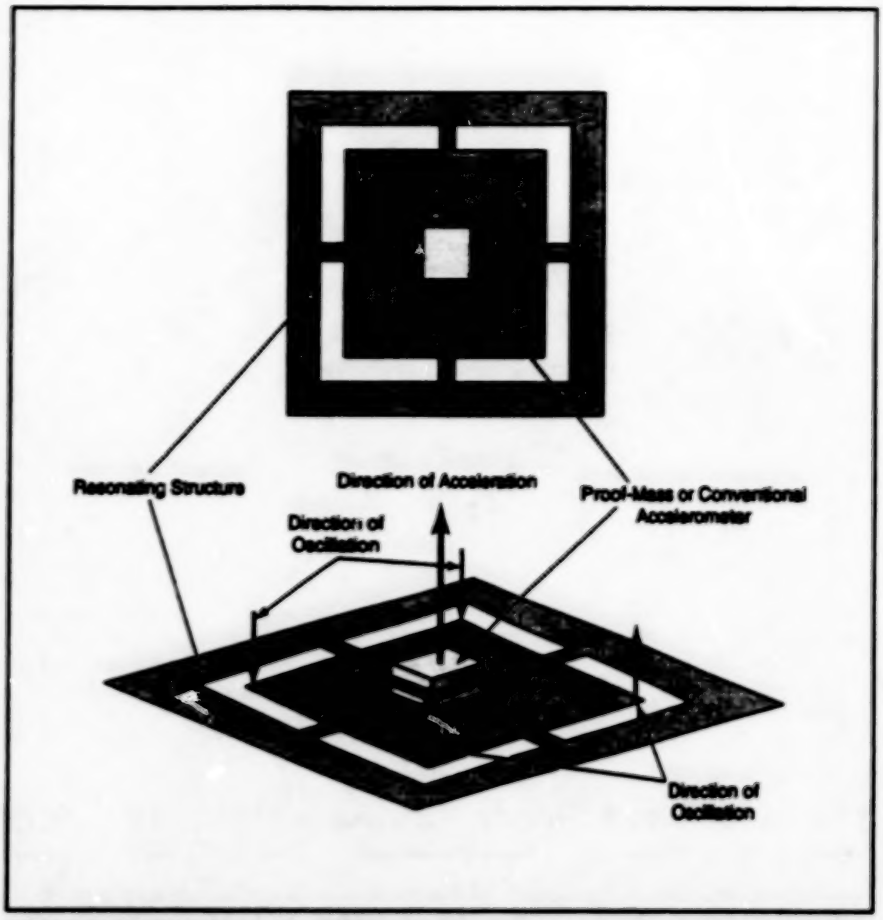

A Micromachined Spring-and-Proof-Mass Accelerometer or a micromachined structure holding a conventional accelerometer would be designed to resonate in a secondary vibrational mode that would be in addition to the primary acceleration-sensing mode. The secondary vibrations would be exploited in a phase-sensitive-detection scheme to increase the sensitivity to acceleration.

Micromachined Planar Vibratory Sensors With Mode Matching

Sensitivity would be increased by exploiting two resonances at the same frequency.

NASA's Jet Propulsion Laboratory, Pasadena, California

Matching of the resonance frequencies of vibrational modes has been proposed as a means to enhance the performances of micromachined planar vibratory sensors and, in particular, of sensors like those described in "Micromachined Planar Vibratory Microgyroscopes" (NPO-19713), page 39. The concept of matching resonances in vibratory sensors is not entirely new; as reported in the cited prior article, this concept is essential to the proper functioning of vibratory microgyroscopes of older design. What is new about the present proposal is taking advantage of both the mode-matching concept and the inherent advantages of micromachined vibratory sensors to achieve unprecedented degrees of responsivity.

To recapitulate from the cited prior article: a typical micromachined planar vibratory microgyroscope (see figure) includes four planar silicon plates connected together in a pattern resembling that of a clover leaf. The plates are suspended by four silicon slab cantilever springs. Plates A and C are driven electrostatically out of phase to oscillate in rocking (seesaw) mode in the z direction. In the absence of other disturbances, plates B and D remain stationary.

One seeks to measure rotation about the z axis. When such rotation occurs, the Coriolis force causes plates B and D to also oscillate in a rocking mode in the z-direction; that is, the Coriolis force causes a transfer of energy from A-C (input) rocking mode to the B-D (output) rocking mode. By use of capacitive proximity sensors, the displacements of plates B and D are measured to obtain data from which the rate of rotation can be inferred.

The mode-matching concept involves the following reasoning: If plates A and B were driven at the resonance frequency of the A-B rocking (input) mode, the A-B rocking motion would effectively be amplified by the resonance quality factor (Q) of that mode. If plates A through D and their supporting cantilever springs were fabricated precisely with fourfold symmetry in the x-y plane, then the two rocking modes would have the same shape, would be oriented orthogonally to each other in the x-y plane, and would have equal resonance frequencies. Because of this mode matching, the B-D (output) rocking motion would also be

30

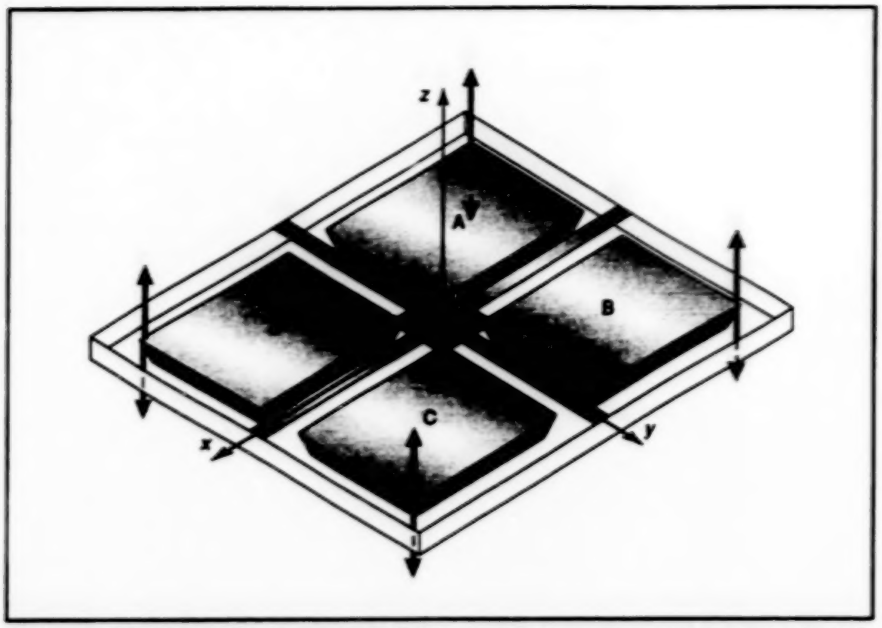

Symmetry Would Result in Degeneracy (that is, equality of resonance frequencies) of the A-C and B-D rocking (seesaw) vibrational modes, which would be coupled slightly by the Coriolis acceleration associated with rotation about the *z* axis. As a result of the mode matching, both modes would be effectively amplified by *Q*.

effectively amplified by *Q*. Inasmuch as the *Q* of a typical micromachined silicon vibratory device can exceed 50,000, the net result would be a large increase in the responsivity of the device.

The precisely symmetrical configuration would offer two additional advantages. First, the resonating structure would be perfectly balanced, with a fixed center of gravity where the sum of forces and moments resulting from vibrations in the two modes could be zero. This would make for low dissipation of energy and thus high *Q*. The second advantage would be that perfect symmetry would preclude differential thermal expansion and thereby preserve the degeneracy of the two vibration modes at all temperatures.

This work was done by Tony K. Tang, William J. Kaiser, and Roman C. Gutierrez of Caltech for **NASA's Jet Propulsion Laboratory**. *No further documentation is available.*
NPO-20048

Micromachined Silicon Vibratory Three-Axis Accelerometer

Several advantageous features would be combined in a single device.

NASA's Jet Propulsion Laboratory, Pasadena, California

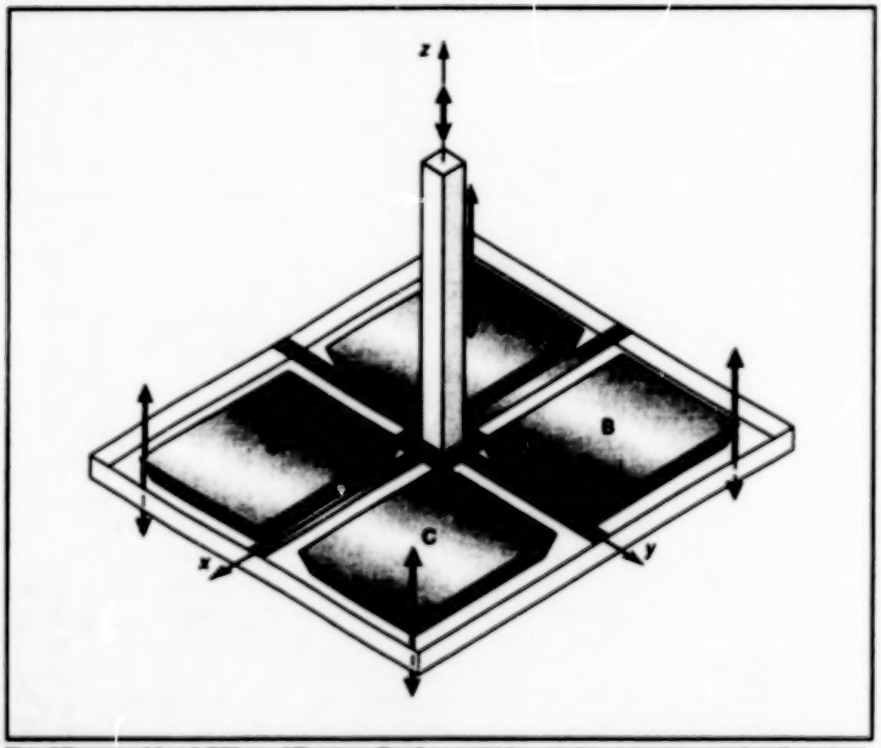

This Micromachined Silicon Vibratory Device could be used to measure acceleration along the *x*, *y*, and *z* axes.

The figure illustrates a proposed micromachined vibratory three-axis accelerometer. This device would include a micromachined silicon vibratory substructure in the *x*-*y* plane, similar to that described in the second of the two preceding articles, "Micromachined Planar Vibratory Sensors With Mode Matching" (NPO-20048). In addition, a rigid rod oriented along the *z* axis would be attached to the center of the vibratory substructure. This device would superficially resemble the rotation-sensing device described in "Planar Vibratory Microgyroscope: Alternative Configuration" (NPO-19714), page 40, but its design would be optimized for sensing translational acceleration instead of rotation.

Electrodes for electrostatic excitation of vibrations and other electrodes for capacitive sensing of vibrational displacements of plates A, B, C, and D would be located under these plates. All four plates and the rod would be driven synchronously at the resonance frequency of the fundamental *z*-axis vibrational mode of the structure. To enhance the signal-to-noise ratio, the capacitance readings would be taken with the help of lock-in amplifiers synchronized by the resonant vibration-exciting signal as described in the first of the two preceding articles, "Modulation/Detection Technique for Measuring Acceleration" (NPO-20049).

In the presence of a positive acceleration along the *x* or the *y* axis, the rod would tilt toward the negative *x* direction or negative *y* direction, respectively, giving

rise to a corresponding tilt of plates A through D. In turn, the tilt of the plates would result in a change in the oscillatory capacitance readings, which could be processed into *x*-axis or *y*-axis acceleration via predetermined relationships among accelerations, tilts, and capacitances. For acceleration along the *z* axis, similar considerations would apply, except that the rod would not tilt; instead, the rod would function as a simple proof mass, and the capacitance readings for all four plates would be indicative of the common *z*-axis oscillation superimposed on the *z*-axis acceleration.

The proposed accelerometer would offer several advantages beyond those explicitly stated above:

- Like micromachined accelerometers in general, this one would have a long operational life and could be made to have relatively large masses suspended by relatively soft springs, with resultant low resonance frequencies and large responses with low damping and low thermal noise.
- The four plates and the space underneath them provide ample surface area for electrostatic-excitation and capacitive-displacement-sensing electrodes; this makes it possible to obtain larger capacitance signals and to use smaller excitation voltages than would otherwise be practical.
- Like other micromachined devices with electrostatic deflection, this device would consume very little power.
- Like micromachined devices in general, this device would be compact and amenable to mass production at low cost per unit.

With design parameters chosen to take maximum advantage of these characteristics, it should be possible to manufacture devices of this type to measure accelerations as small as about 10^{-8} m/s^2.

This work was done by Tony K. Tang, Roman C. Gutierrez, Wen J. Li, Christopher Stell, Jaroslava Wilcox, and William J. Kaiser of Caltech for **NASA's Jet Propulsion Laboratory**. *No further documentation is available.*
NPO-20047

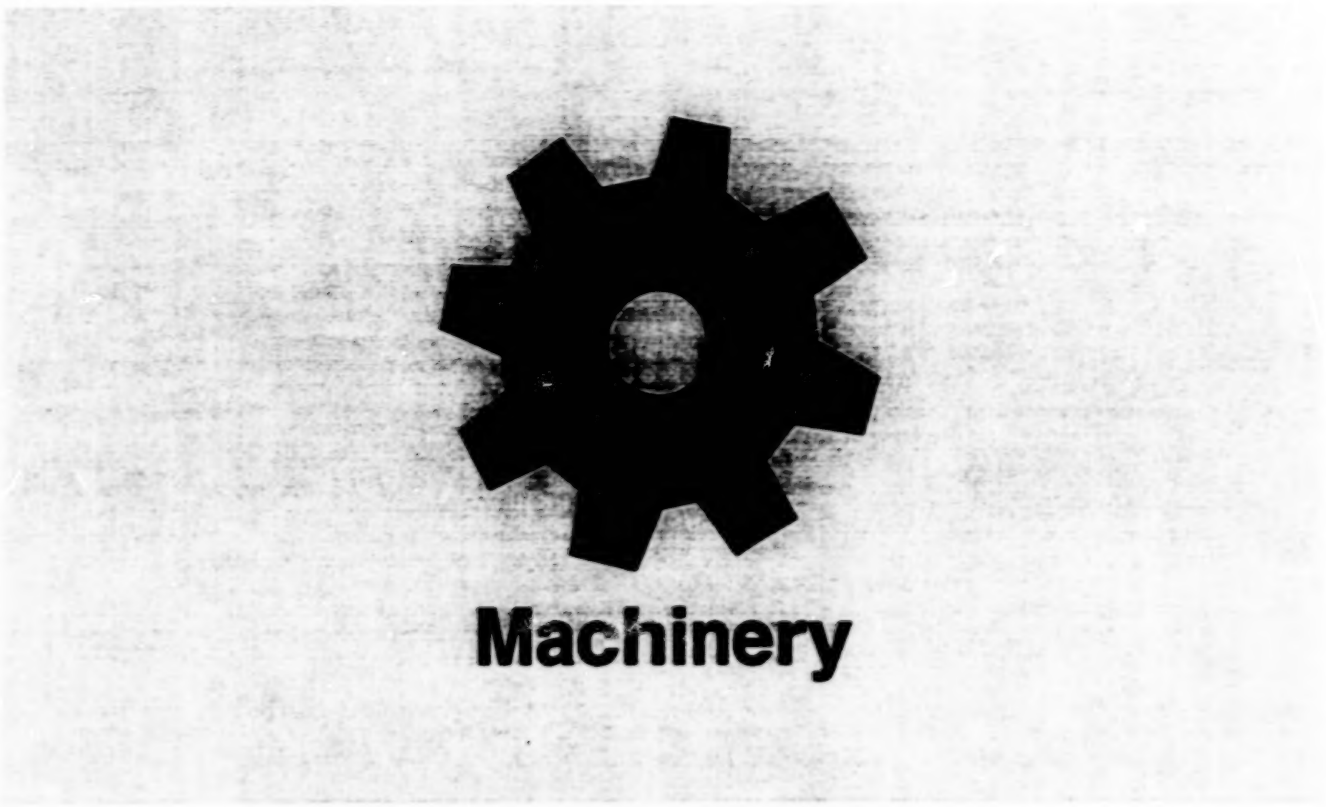

Machinery

Hardware, Techniques, and Processes

47 Miniature Instrumented Robotic Vehicles for Exploration

Miniature Instrumented Robotic Vehicles for Exploration

Components would perform multiple functions, maximizing utilization of mass.

NASA's Jet Propulsion Laboratory, Pasadena, California

Toy-sized, instrumented, automated or remotely controlled robotic vehicles called "nanorovers" have been proposed for use in exploration of Mars and the moons of the outer planets. Terrestrial versions could be devised for such uses as monitoring toxic waste dumps and exploring terrain in harsh environments like those in craters of volcanoes and in polar regions. It should also be possible to build simplified toy versions.

These nanorovers would differ from the ones described in "Tetherless, Optically Controlled Nanorovers" (NPO-19605), *NASA Tech Briefs*, Vol. 21, No. 3 (March 1997), page 92. The nanorovers according to the present concept would feature four-wheel drive actuated by miniature commercially available gearmotors, with rocker bogie suspensions (see figure). A nanorover would incorporate several scientific instruments plus all necessary power, communication, and control electronic circuitry. The scientific instruments could include a video camera with a focusing mechanism to accommodate a range of distances and resolutions, a point scanning infrared spectrometer and a mass spectrometer for identifying materials in rocks or other nearby objects, and several laser diodes that emit at different wavelengths.

Despite the multiplicity of instruments and functions, the overall dimensions of a typical nanorover would be only a few centimeters, and its overall mass would be of the order of 100 g. Such an extreme combination of miniaturization and versatility would be achieved by utilizing the best commercially available components and

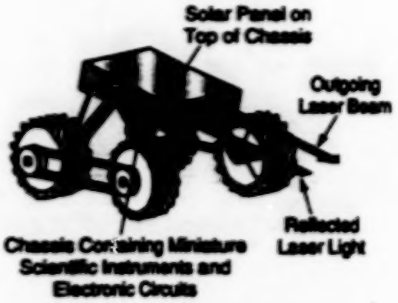

A Nanorover, resembling a toy all-terrain vehicle in shape and size, would feature a sophisticated mass- and space-efficient design for implementing multiple scientific, navigation, and control functions.

materials in an advanced design in which structures and functions that have traditionally been designed according to different disciplines and assigned separate functions would be combined and intercoupled. In other words, each structural component, each electronic component, each actuator, and each sensory component would be designed to perform as many different functions as possible so that mass and size allowances would not be used up any more than necessary. This concept of multiple functionality is best explained by the following examples:

- The main structural components of the vehicle chassis would be two printed-circuit boards, between which all electronic circuitry would be mounted. These boards would also serve as a bench for the scientific instruments, and the top surface of the upper board would serve as a platform for solar photovoltaic cells.
- The mechanism for adjusting the camera focus would also be used to scan the infrared spectrometer over its wavelength range.
- The laser diodes would provide excitation for the spectrometer. Reflected laser light would also provide feedback for a piezoelectric actuator for fine adjustment of a spectrometer slit. One of the laser diodes operating at more than its usual power would be used to vaporize surface material from a rock or other object to expose fresh, uncontaminated underlying material for analysis by the infrared spectrometer. Alternatively or in addition, vaporized material could be analyzed by the mass spectrometer.
- Being tilted with respect to the local terrain, the panel of solar cells would generate maximum power when aimed in azimuth approximately toward the Sun. Thus, in addition to generating power, the solar panel would provide an approximate direction reference for navigation. For this purpose, the navigation routine would include occasional pirouettelike maneuvers.

This work was done by Brian Wilcox, Annette K. Nasif, Michael A. Newell, Jan A. Tarsala, and Sarita Thakoor of Caltech for **NASA's Jet Propulsion Laboratory.** *Further information is contained in a TSP [see page 1].*

NPO-19946

34

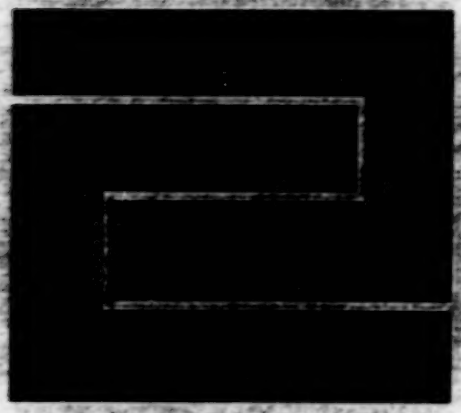

Fabrication Technology

Hardware, Techniques, and Processes

51 Setup for Multidirectional Wire EDM

51 Noncontact Automatic Standoff Control for Arc Welding

Setup for Multidirectional Wire EDM

Large workpieces can be cut along multiple planes.

Marshall Space Flight Center, Alabama

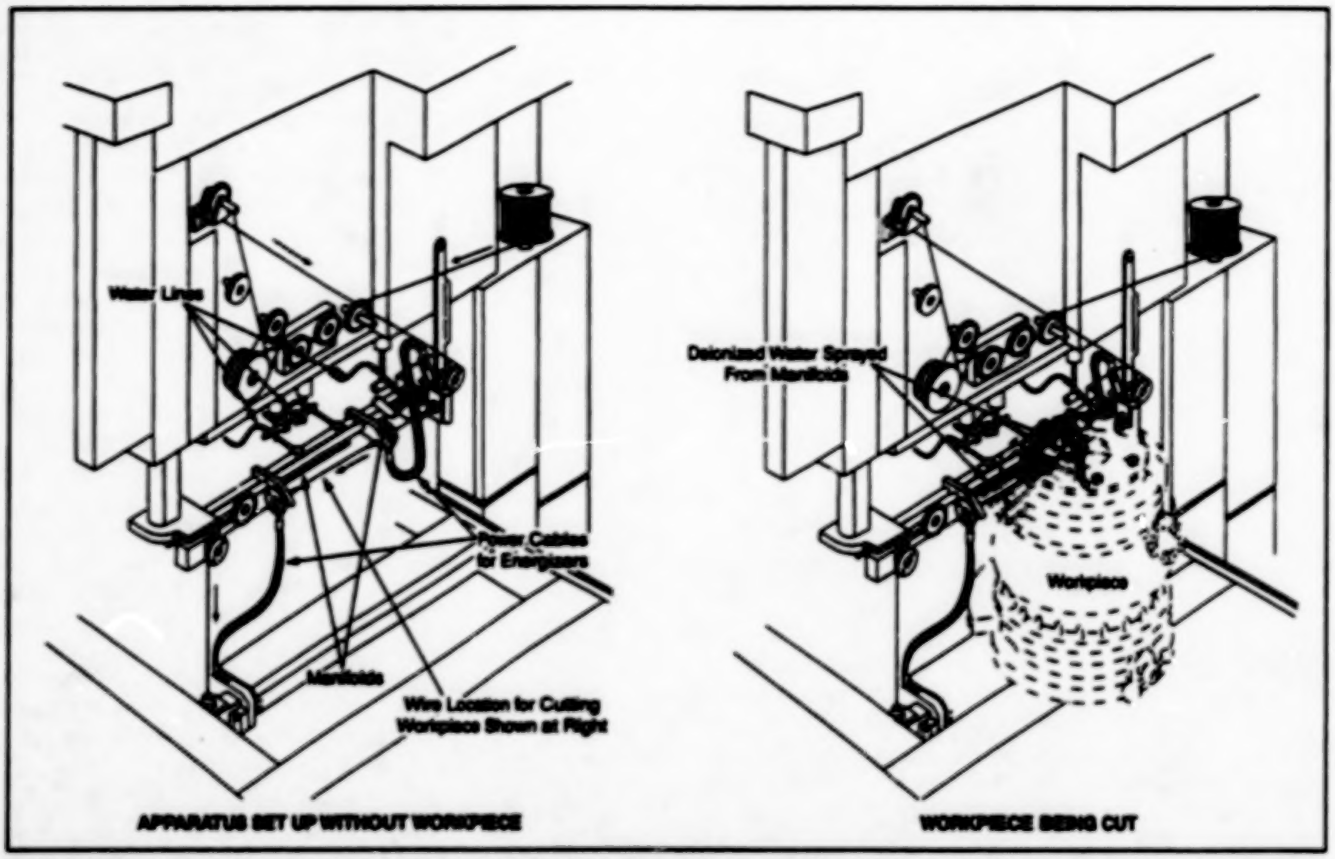

Multiple Pulleys are used to position and orient the wire in the plane along which the workpiece is to be cut. In this case, the workpiece (a turbopump) is rotated continuously past the cutting location on the wire. The sprays of deionized water cool the workpiece.

An apparatus for wire electrical-discharge machining (EDM) includes a compound-pulley mechanism for routing the wire in various directions, making it possible to cut a workpiece in multiple planes, one plane at a time. For example, when set up as shown in the figure, the apparatus can be used to cut through the wall of the workpiece along a horizontal plane that starts out as a wire line tangent to the round outer surface of the workpiece at the desired height. During EDM, the workpiece can be rotated about its vertical axis by use of a turntable, so that the cut through the wall can be extended along the entire circumference, without cutting any parts inside the workpiece.

The pulley spools are made of electrically insulating material (nylon). The pulleys are parts of a mechanism that holds the wire in the specified position and at the specified tension. The wire is longer than that used in typical other EDM apparatuses and excessive voltage drop could arise from EDM current flowing in the longer wire. Therefore, it is desirable to supply the current as close as possible to the cutting location; this is done by making electrical contact between the wire and the source of EDM power not only at an end of the wire but also via carbide blocks, called "energizers," against which the wire brushes at several locations.

This work was done by Gary N. Booth, R. Michael Malinzak, and Gareth L. Simpson of Rockwell International Corp. for Marshall Space Flight Center. Further information is contained in a TSP [see page 1].
MFS-30115

Noncontact Automatic Standoff Control for Arc Welding

The standoff distance would be monitored optically.

Marshall Space Flight Center, Alabama

A proposed noncontact method of automatic standoff control (ASOC) for arc welding is based on optical monitoring of the standoff distance; that is, the distance between the welding torch and the workpiece. Two previously reported methods of ASOC involve the use of mechanisms in contact with the workpiece [see "Automatic Stand-Off Control for Arc Welding" (MFS-28294), *NASA Tech Briefs*, Vol. 20, No. 9 (September 1996), page 90]. All of these methods of ASOC have been investigated in efforts to find alternatives to an older automatic-voltage-control (AVC) method, which was found to be unsatisfactory because the welding-arc voltage is not simply proportional to the standoff distance, but can fluctuate even when the

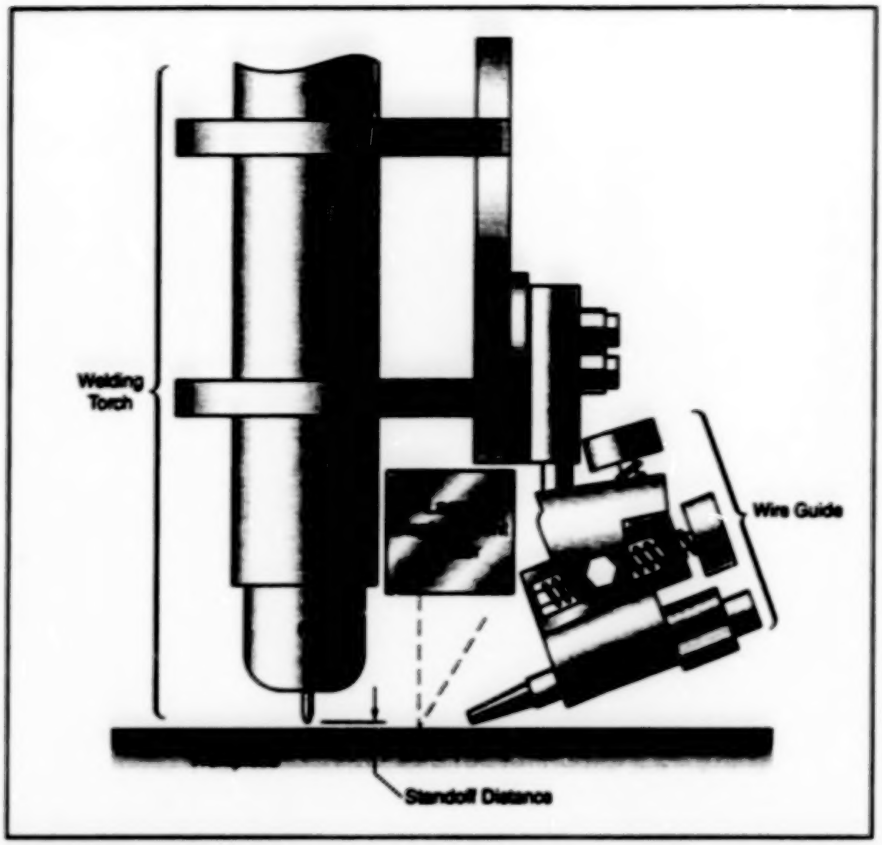

A Laser Displacement Sensor would monitor the standoff distance, providing a feedback signal for maintaining the standoff distance within a narrow range.

standoff distance remains constant, and can give a false distance reading at startup.

In the proposed noncontact method of ASOC, an industrial laser displacement sensor would be installed on the welding-torch assembly and used to monitor the standoff distance. The sensor could be, for example, a commercial unit that measures displacement relative to a reference distance, generating an analog output signal indicative of the displacement every millisecond. The unit is designed to be capable of measuring to a resolution of 2 μm within a range of ±5 mm about a reference distance. The displacement output of the sensor can be set to zero at the reference distance.

The output of the sensor would be processed through a proportional+integral+derivative (PID) signal-processing circuit in an automatic-welding-control system (AWCS) to obtain a feedback control signal for adjusting the height of the welding torch above the workpiece. Because the AWCS was designed for AVC, original PID parameters were chosen to optimize the response of the torch-positioning servocontrol subsystem to the arc voltage. In implementing the proposed method, it would be necessary to modify the PID parameters to optimize the response to the output of the laser displacement sensor. It has been estimated that this method would enable control of the standoff distance to an accuracy of 0.007 in. (0.18 mm).

This work was done by Richard Venable of Lockheed Martin for **Marshall Space Flight Center.** *Further information is contained in a TSP [see page 1].*
MFS-31171

37

Mathematics and Information Sciences

Hardware, Techniques, and Processes

55 Using Machine Learning To Study Aircraft Control Stability

38

Using Machine Learning To Study Aircraft Control Stability

Dynamical simulations are performed and analyzed in a genetic-algorithm-based search.

Dryden Flight Research Center, Edwards, California

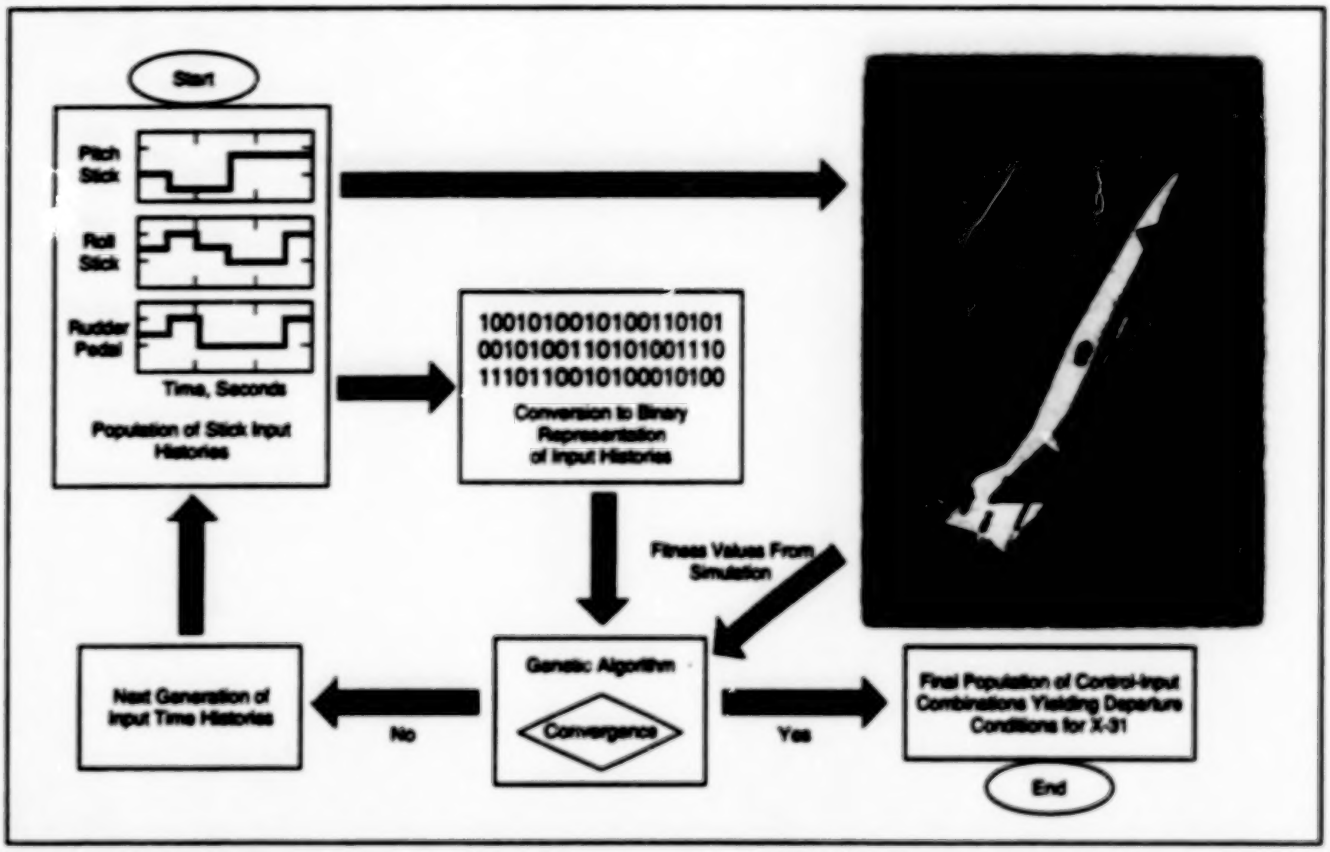

The Computational Departure-Resistance-Evaluation Process consists mostly of a genetic-algorithm-based search among dynamical simulations — in this case, simulations of responses of the X-31 airplane to various combinations of time-varying control inputs.

Machine learning techniques have been utilized in research on flight-control stability and instability in advanced fighter-type airplanes. To give meaning to a description of this research, it is necessary to define some terms: In this context, "departure" signifies instability and/or uncontrollability in the response of an aircraft to flight-control actions at a given flight condition; "departure susceptibility" means susceptibility of an aircraft to departure — that is, to flight-control instability and/or uncontrollability; and "departure resistance" signifies resistance to departure — that is, stability and controllability in the response of an aircraft to flight-control actions at a given flight condition.

Departure-resistance testing of such highly complex and maneuverable aircraft as modern fighters is difficult and presents a challenge for engineers. As aircraft have become more complex and maneuverable, departure susceptibility has increased. Increases in the complexity of aircraft systems have also made it more difficult to "wring out" these systems to find potential pitfalls; this is evidenced by the number of incidents in the recent history of modern fly-by-wire aircraft. To ensure a level of safety, a typical aircraft is flown within a safe margin of conditions that could lead to a departure, reducing the available maneuvering envelope (the allowable limits of control actions, velocities, and attitudes during maneuvers) of the aircraft. Such margins of safety are found by performing simple, single-parameter static- and dynamic-stability-prediction simulations and/or by flight testing.

Some examples of simple, single-parameter criteria include those based on (1) $C_{n\beta}dyn$, the dynamic-directional-stability parameter, and (2) the lateral-control-departure parameter (LCDP). These criteria are useful for predicting departure characteristics, but their accuracies may be limited because of simplifying assumptions made in their mathematical derivations. They have not exhibited consistent correlation with results from flight tests at high angles of attack. Also, the information obtained from simulations and flight tests of departure-resistance maneuvers can be limited in that the number of conditions tested is necessarily small in comparison with the total number of possible conditions. The coupling of (1) an infinite number of possible flight conditions and control-input combinations with (2) the complex architectures of modern control systems makes it difficult, at best, to search for possible problem areas in the flight envelope. The limitations of prediction methods of both types increase at high angles of attack, where aircraft dynamics become more complex and aerodynamic effects are nonlinear. Because of the limitations of these methods, NASA is using machine-learning techniques in research directed toward improving on methods of predicting departure resistance.

In support of flight tests of the X-31 airplane at Dryden Flight Research Center, machine learning techniques have been used in computer simulations (see figure) in which one searches for control-input strategies that result in uncontrollable conditions. A genetic algorithm generates quasi-random stick

inputs for a high-fidelity X-31 engineering simulation. Each input is evaluated to determine whether it causes the airplane to exceed flight-control limits or whether the states of the airplane become uncontrolled. The genetic algorithm then uses the results of each search iteration and "learns" what types of control-input strategies could lead to departed flight conditions. A major benefit of this automated search is that a very large set of control inputs and flight conditions can be tested without interaction with a pilot. The result of the genetic-algorithm-based search is a final population, or set, of control-input combinations at various points in the flight envelope that lead to potential departures. In addition, the search can reveal aspects of flight-control logic that one might need to analyze further. Once potential departures or problem areas are located in the search, one can conduct a test in which a pilot attempts to duplicate the control inputs or maneuvers in question.

An example of a departure found during such a genetic search is one due to inertial coupling in the X-31 pitch axis. Inertial-coupling departures have been seen during other flight-test programs; they are typical of highly agile fighter airplanes with small roll and large pitch moments of inertia. An inertial-coupling departure occurs when a pilot or automatic-flight-control logic is unable to compensate for inertial effects caused by a rapid, cross-axis maneuver. For example, inertial coupling occurs during rapid rolls and roll reversals performed in conjunction with rapid changes in pitch. The inertial-coupling departure located by the genetic search with the X-31 simulation occurred when multiple rolls at low angles of attack were performed with changes of pitch from negative to positive angles of attack. During the departure, pitch control and lateral directional control could not overcome the inertial coupling in the pitch axis. Such maneuvers could occur during air combat, when oblique turns are performed and pilots frequently change maneuver plane of the aircraft in efforts to aim weapons. Because of the discovery of the inertial-coupling departure in the genetic search and simulation, and because inertial-coupling incidents had been observed in other flight-test programs, multiple rolls at low angles of attack were prohibited during flight test of the X-31.

Another example of a departure located by genetic search includes one, found during expansion of the X-31 flight envelope, caused by asymmetries in aerodynamics. Though there are slight differences and simplifications between the simulation models and the real aircraft, the results of this research have shown that it is possible to use machine-learning techniques to identify potential controllability problems that can later be verified or avoided during flight test.

This work was done by Wes Ryan of PRC, Inc., for **Dryden Flight Research Center**. *Further information is contained in a TSP [see page 1].*
DRC-95-38

40

END

03-17-98